OAK RIDGE NATIONAL LABORATORY

operated by

UNION CARBIDE CORPORATION

for the

U.S. ATOMIC ENERGY COMMISSION

UNION CARBIDE

ORNL- TM- 1038

CALCULATED TISSUE CURRENT-TO-DOSE CONVERSION FACTORS FOR

NUCLEONS BELOW 400MeV

C. D. Zerby
W. E. Kinney

Contract No. W-7405-eng-26

NEUTRON PHYSICS DIVISION

CALCULATED TISSUE CURRENT-TO-DOSE CONVERSION FACTORS FOR
NUCLEONS BELOW 400 MeV*

C. D. Zerby** and W. E. Kinney

MAY 1965

OAK RIDGE NATIONAL LABORATORY
Oak Ridge, Tennessee
operated by
UNION CARBIDE CORPORATION
for the
U.S. ATOMIC ENERGY COMMISSION

iii

TABLE OF CONTENTS

Page No.

ABSTRACT 27877

To assist in the evaluation of the hazard associated
with exposure to high-energy neutrons or protons, a series
of Monte Carlo computer programs were used to calculate
the energy deposition that results from high-energy inci-
dent nucleons as a function of depth in a slab of tissue.
The programs included nonelastic and elastic interactions,
as well as evaporation processes and nuclear recoils. A
30-cm-thick infinite slab of tissue was treated, and cases
of normal and isotropic incidence of 400-, 300-, 200-, 100-,
and 60-MeV protons and neutrons were computed. From these
data current-to-dose conversion factors were extracted for
the average-whole-body, the 5-cm-depth, the surface, and
the maximum doses. A set of quality factors (QF's) was
adopted for transforming rad dose to rem dose, but de-
tailed energy-deposition data are also presented so that
any preferred set of QF's can be used to obtain estimates
of the rem dose.

I. INTRODUCTION

To assess the hazard to personnel encountering high-energy radiation in space or near accelerators, it is necessary to have a means of estimating the biological effects of these radiations. A useful and simple way of obtaining such an estimate is to multiply the current of a given type of incident particle by the appropriate current-to-dose conversion factor to obtain a measure of the dose received. Of course the physiological effects of radiation can be determined only by experiment, but in the past these effects have been successfully correlated with the dose from low-energy radiations. Hence, it is expected that a correlation can also be found between the physiological effects and the dose from high-energy radiations, although it may be more complicated. To facilitate such possible correlations a series of Monte Carlo calculations have been carried out to determine many details about energy deposition by high-energy neutrons and protons in tissue as a function of depth. From these data, rad doses (1 rad = 100 ergs/g) and rem doses (rem = roentgen equivalent man) were calculated, and current-to-dose conversion factors for the dose at the surface of the body, the dose at a depth of 5 cm, the average-whole-body dose, and the peak dose were extracted for hazard evaluation. The incident-nucleon energies considered were from 60 to 400 MeV.

The model of the body selected was a 30-cm-thick infinite slab of tissue which was uniformly exposed to the radiation over one face. Both normally incident and isotropically incident radiations were calculated in an effort to bracket the dose that would be received with some intermediate angular distribution.

Previous calculations of the tissue dose from high-energy radiations have been made by Neary and Mulvey,[1] who estimated maximum permissible fluxes of nucleons in the 40- to 1000-MeV energy range on the basis of rather qualitative considerations, and by Turner et al.,[2] who performed more detailed Monte Carlo calculations of the tissue dose due to incident protons up to 400 MeV. The present calculation, which is described in detail in Section II, is an independent extension of the latter study. It includes nonelastic interactions of the nucleons with nuclei and takes into account the contribution of cascade particles and nuclear evaporation particles up through the alpha particle. Energy loss by elastic collisions of low-energy neutrons is also accounted for, as well as the transport of these particles.

Since the method of converting energy deposition to rem dose will be subject to change as additional data become available, it was suggested[3] that a separate calculation be made of the energy deposition by the protons as they passed through various energy ranges at the various depths. In this way any preferred set of quality factors (QF's) can be applied with relative ease. This was done in the calculation as described in Section II. Information about energy deposition by heavy recoils and heavy charged particles was also computed and is reported separately for the same reason.

Experimental data on the tissue dose due to high-energy radiation are very scarce. The experiment of Shalnov[4] is an isolated example of the measurement of the dose from high-energy neutrons. His data include the dose as a function of depth in tissue-like material from approximately 140-MeV neutrons stripped from 280-MeV deuterons on copper and from a broad spectrum from charge-exchange reactions of 480-MeV protons on beryllium.

The results of the present calculation are compared with those of the previous calculations and with Shalnov's experimental data in Section III. A detailed breakdown of the energy deposition data is reported in Section IV for the depths and conditions corresponding to those for which the current-to-dose conversion factors were calculated. (Additional details are reported elsewhere.[5]) Section IV also gives the current-to-dose data, and a few final comments are contained in the concluding Section V.

II. METHODS

The interaction of a high-energy nucleon with matter initiates a complex avalanche of lower energy secondary particles which proceed through the medium, increasing in population and decreasing in total energy as energy is deposited in the medium. In general, a nonelastic interaction of a nucleon with a nucleus produces, first of all, several secondary nucleons which are due to direct interactions of the incident particle with the nuclear constituents and which have energies ranging from a few MeV up to a large fraction of the incident-particle energy. The recoiling nucleus is left in a highly excited state and rids itself of most of its excess energy by evaporating additional nucleons and heavy particles of relatively low energy, of the order of a few MeV. Any energy left after evaporation presumably goes into the production of electromagnetic radiation.

A series of Monte Carlo programs[6] for the IBM-7090 computer has been written for the study of the transport of nucleons of energies up to 400 MeV through quite arbitrary geometrical configurations.[*] The calculations are divided into two parts, those above 50 MeV being performed separately since at lower energies the model used for computing intranuclear cascades is of doubtful validity and neutron transport requires a more complex treatment.

The calculation begins with the selection of a source nucleon from the desired energy and angular distributions. Once a source particle is selected, a flight distance to a position where a nuclear interaction might occur is chosen from the exponential distribution with total macroscopic

---

[*]Copies of the codes and instructions in their use may be obtained from the Radiation Shielding Information Center, Oak Ridge National Laboratory, Post Office Box X, Oak Ridge, Tennessee, 37831.

geometric mean free path. (The n,p cross section at 50 MeV is used as a geometric cross section for hydrogen.) If the nucleon is a proton, its energy at the end of the flight is determined by means of range tables computed from the stopping-power formula for ionization energy loss.[7] Then, a target nucleus is selected from the constituents of the medium, and if it is not hydrogen, the energy and type of incident nucleon, along with the charge and mass numbers of the target nucleus, are given to a sub-routine version of Bertini's intranuclear cascade code.[8] If the target is hydrogen, an elastic n,p or p,p scattering is allowed to take place with probability equal to the ratio of the elastic scattering cross section to the "geometric" cross section (the n,p elastic scattering cross section at 50 MeV). In the event that the scattering does not take place, another flight distance is selected and the nucleon is moved straight ahead from its present position.

The intranuclear cascade subroutine is itself a Monte Carlo transport calculation on an intranuclear scale. Free-particle n,p and p,p cross sections and angular distributions are assumed to hold for the calculation of the interaction of the incident nucleon with the nucleons of the nucleus. The nucleon may pass directly through the nucleus with no interaction whatsoever, in which case another flight distance is chosen, the particle is moved straight ahead from its present position to the next possible interaction site, and another attempt at a nuclear interaction is made. The transport is thus continued until the nucleon disappears in a nuclear interaction, leaks from the system, or, in the case of protons, slows down past 50 MeV.

As the nucleon is traced through the nucleus by Bertini's subroutine, it collides with at least one nucleon of the nucleus with a probability equal to the ratio of nonelastic cross section to the geometric cross

7

section. The target nucleons, upon recoil, may in turn collide with other nucleons, thus giving rise to an intranuclear cascade. Some nucleons may be knocked out of the nucleus, leaving behind a highly excited residual nucleus whose excitation energy is tabulated for later use in the evaporation process. If such a nuclear interaction occurs, then the products of the reaction are transported through the medium just as the initiating particle was. The details of each event in a particle's life such as a nuclear interaction, crossing of a spatial boundary, or slowing down past 50 MeV, are recorded on magnetic tape for later analysis.

When the desired number of source particles and their progeny have been traced, an analysis code reads the magnetic tape containing the nucleon histories and analyzes for the desired nucleon distributions. This code completes the intranuclear cascade by evaporating additional nucleons from the highly excited nuclei by means of an evaporation subroutine written by Dresner,[9] which is essentially the same as one written by Dostrovsky et al.[10] This subroutine utilizes evaporation theory to compute probabilities for the emission of neutrons, protons, deuterons, tritons, ^{3}He nuclei, and alpha particles, the probabilities being functions of the excitation energy, the charge, and the mass of the excited nucleus. The particle to be emitted is chosen and its energy is selected from a Maxwell-Boltzmann distribution having a nuclear temperature appropriate to the excited residual nucleus. It then carries away this kinetic energy along with its binding energy, leaving a new residual nucleus with a lower excitation energy. The evaporation continues as long as there is enough energy to emit a particle. Any residual excitation energy left after all the particles have been evaporated presumably is expended in gamma-ray emission.

Another subroutine in the analysis code analyzes all protons with energies below 50 MeV which may have resulted from evaporation or from direct interaction with the nucleus, as well as those protons which have slowed down below this energy. The assumption was made in this study that these protons proceeded straight ahead to the end of their range without suffering nuclear interaction (2.2 cm for 50-MeV protons in tissue of our assumed composition). This should cause little error in the calculation. Parameters associated with neutrons appearing below 50 MeV are put on a magnetic tape which is used later as a source tape for a low-energy (< 50-MeV) neutron transport calculation. Particles of mass greater than 1, including evaporated heavy particles and recoiling nuclei, were assumed to deposit their energy at the site of their birth.

The transport of neutrons from energies of 50 MeV down to thermal differs from their transport above 50 MeV in two important respects. First, elastic scattering becomes an important mechanism for energy loss and is, in fact, the only one below roughly 10-100 keV, whereas it may be neglected in the high-energy calculation save for the case of elastic scattering by hydrogen. Second, neutron cross sections below a few MeV are not smooth functions of the energy, and their description requires a large amount of numerical information. The code used for this purpose, known as the O5R, was developed by Coveyou et al.[11] and is notable for its ability to describe cross sections in great detail and for flexibility in the variety of problems it is able to solve.

In other respects the transport is accomplished in much the same way as it is for the high-energy nucleons; The neutrons are introduced,

in this case throughout the medium since they result from nuclear inter-
actions, a flight path is chosen, and a position for an elastic or a non-
elastic collision is computed. A scatterer is selected and, if the scat-
tering is elastic, the neutron continues with reduced energy to a newly
selected collision site and the process is repeated until the neutron dis-
appears from the system by leaking, by slowing down past a low-energy cut-
off, or by being absorbed in a nonelastic event.

In the calculation of elastic scattering it was assumed that the angu-
lar distribution in the center-of-mass system of coordinates could be repre-
sented by a linear function of the cosine of the angle of scattering. This
is not a very good representation for the angular distribution of elastic
scattering from the heavy constituents of tissue above about 1 MeV.[12]
However, most of the neutrons appear with energies of a few MeV and are
rapidly degraded in energy by collisions with hydrogen. Besides, the con-
tribution of the neutrons below 50 MeV to the dose in tissue amounts to
roughly 10% of the total dose when the incident primary nucleons are neu-
trons and to only about 2% when the primary nucleons are protons and there-
fore the assumption should introduce little error.

If the scattering is nonelastic, the event is handled by means of an
abbreviated version of Dresner's evaporation code[9] which boils off neutrons,
protons, and alpha particles only. Neutrons resulting from nonelastic
events such as (n,n') or (n,2n) are transported in turn, just as was the
neutron initiating the event. Each event in a neutron's life, be it an
escape from the system, a slowing down past cutoff energy, or a collision,
is recorded on magnetic tape for later analysis just as is done with the
high-energy nucleons. When all neutrons on the source tape resulting
from the high-energy transport calculation have been processed, an

analysis code reads the magnetic tape containing the neutron histories
and analyzes them to estimate the quantities of interest.

With the hope of arriving at some practical, usable current-to-dose
conversion factors of sufficient generality of application, a 30-cm-thick
infinite slab of tissue was chosen for study of the dose problem. This is
not an unrealistic model for doses in the abdominal region of a man and it
leads to overestimates of the dose in the extremities and head. Moreover,
it is a model which is subject to easy computation and has been used before
in depth-dose studies.[13] The tissue was assumed to have a composition[14]
$C_{21}H_{140}O_{57}N_3$ with a density of 1 g/cm^3, assumptions which result in the
nuclear densities given in Table 1. The average ionization potentials
which were used in the stopping-power formula for the computation of the
range are also listed in Table 1. A straightforward numerical integra-
tion of the inverse of the stopping-power formula for ionization energy
loss gives the range of protons to 1 MeV as a function of energy, as shown
in Fig. 1. The calculated neutron and proton cross sections for nuclear
interaction are shown in Fig. 2 as a function of energy for carbon and oxygen.
The cross sections, which are equal to each other, result from many trials
with Bertini's intranuclear cascade code. The n,p and p,p cross sections
that were used for the calculation of a hydrogen elastic scattering are
also shown.

In the application of the current-to-dose conversion factors it is to
be expected that widely varying angular distributions of nucleons incident
upon the body will be encountered. In order to provide current-to-dose con-
version factors which could be used to estimate upper and lower bounds on
the doses for practical cases of interest, the nucleons were made to impinge
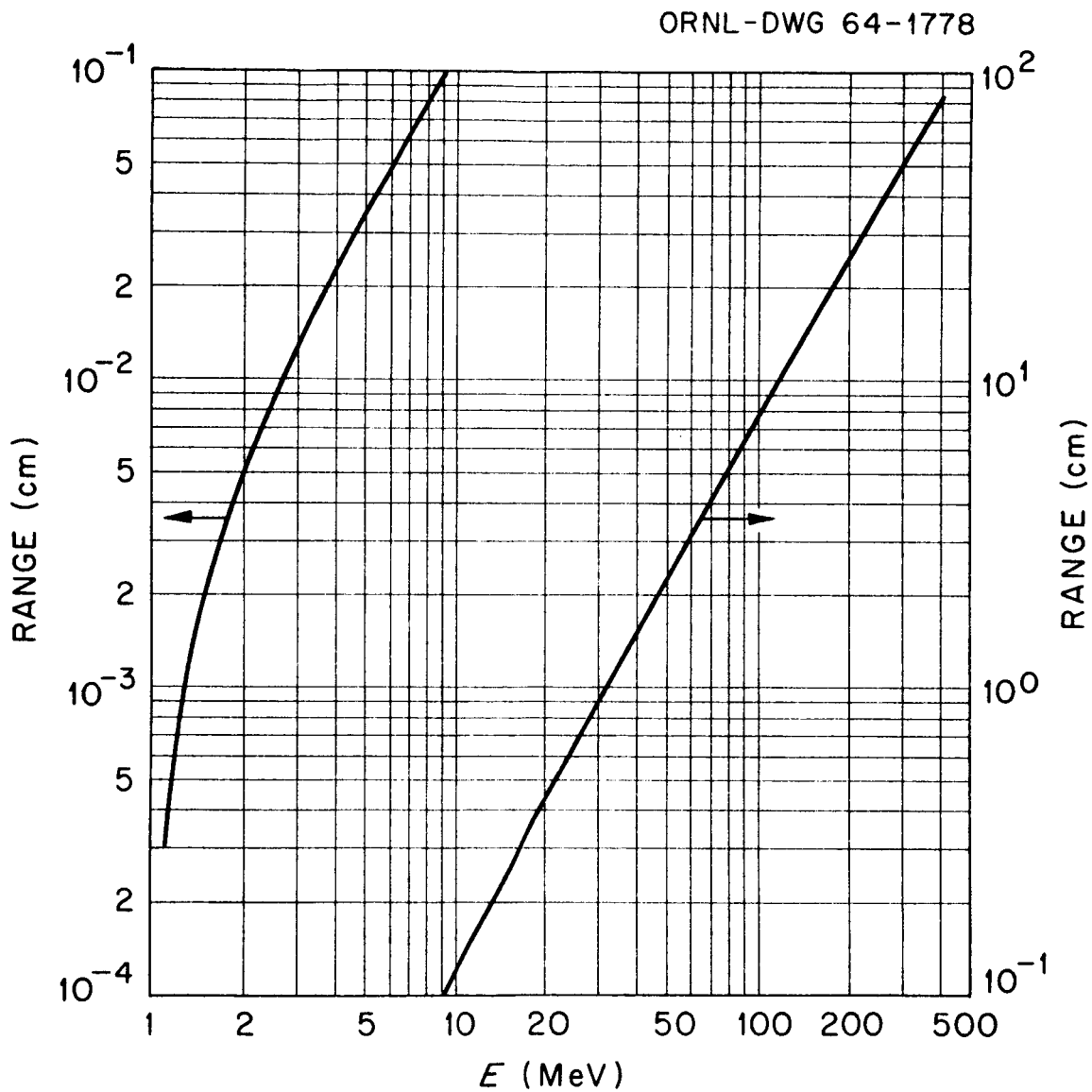
ORNL-DWG 64-1778

Fig. 1.   Range to 1 MeV of Protons in Tissue vs Energy.
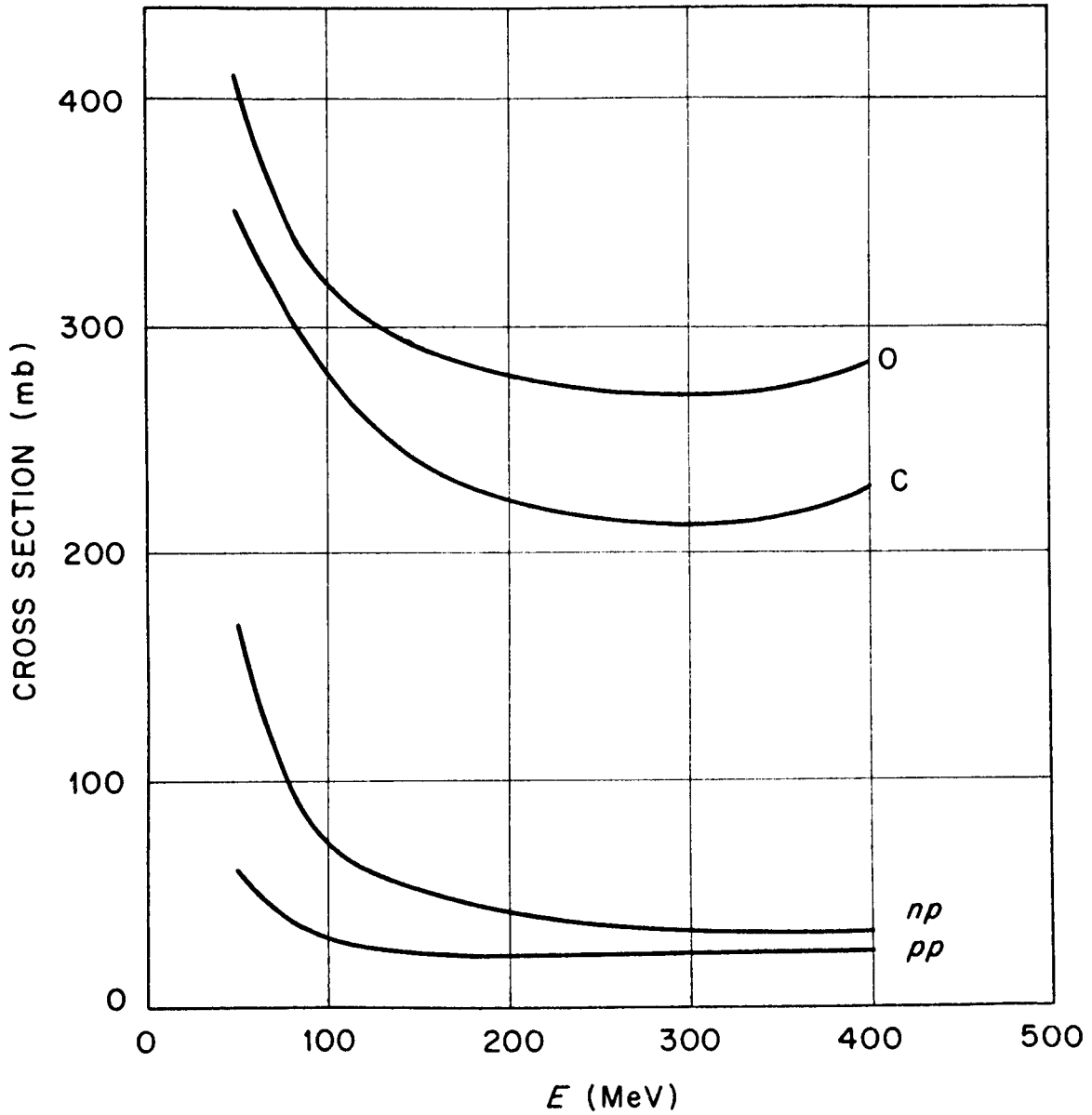
ORNL-DWG 64-1779

Fig. 2. Calculated Nonelastic Nucleon Cross Sections for Carbon and Oxygen from the Intranuclear Cascade Program and n,n and n,p Cross Sections vs Energy.

Table 1

Composition and Mean Excitation
Potentials for Tissue

Element	Nucleon Density [(nuclei/cm^3) x 10^{-24}]	Mean Excitation Potential (eV)
H	6.265 x 10^{-2}	17.5
O	2.55075 x 10^{-2}	99.0
C	9.3975 x 10^{-3}	74.44
N	1.3425 x 10^{-3}	86.0

uniformly over the face of the slab of tissue both normally and isotropically, with the expectation that these two extremes of incident angular distribution would represent the bounding cases. This is discussed further in Section IV. Generally, 10,000 monoenergetic source nucleons were introduced at each of the source energies of 400, 300, 200, 100, and 60 MeV and for each angular distribution. The 30-cm slab was divided into 30 subslabs of 1-cm thickness, and the energy deposited in each subslab due to primary protons, secondary cascade protons, secondary evaporated protons, evaporated heavy (mass > 1) particles, and recoil nuclei resulting from both high-energy nuclear interactions and low-energy neutron elastic collisions was reported. The residual nucleus excitation energy available for gamma-ray production was also recorded in each subslab.

The dose as a function of depth was calculated in units of rads and rems. For the purpose of converting the rad to rem units the energy deposition resulting from protons as they passed through the energy ranges 0-1, 1-5, 5-10, 10-50, and > 50 MeV was recorded separately. For each interval average QF values of 8, 3, 1.25, 1, and 1, respectively, were calculated from the QF vs LET (linear energy transfer) curve shown in Fig. 3. The
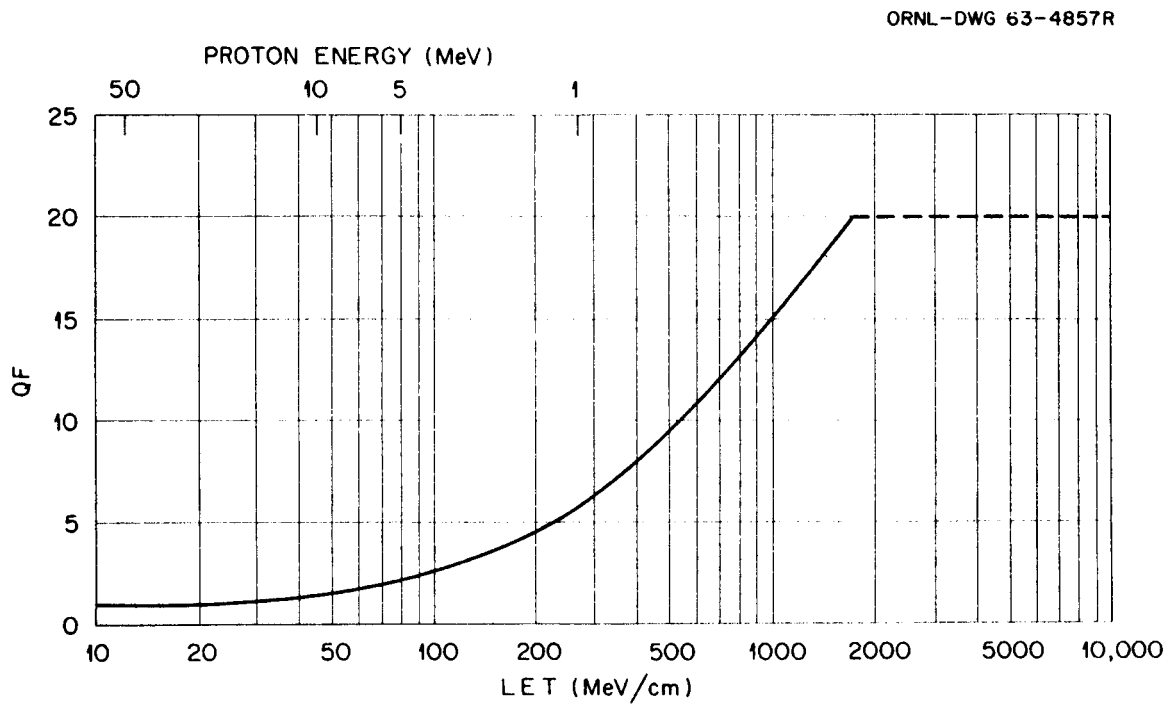
Fig. 3.   QF vs LET Curve.

graphical data were derived from a table in the National Bureau of Standards Handbook 59,[15] which agree very closely with the 1962 recommendations of the RBE committee to the ICRP and ICRU.[16] The values of the energy of the proton shown in Fig. 3 were correlated with the LET by means of the stopping-power formulas. The average values of QF in the interval (E_1, E_2) quoted above were calculated from the relation

$$Av\ QF = (E_2 - E_1)^{-1} \int_{E_1}^{E_2} R(E)\ dE \quad ,$$

where $R(E)$ is the QF expressed as a function of energy.

The constant value 20 for QF above an LET value of 1750 MeV/cm shown in Fig. 3 is not from Handbook 59 but constitutes a quite arbitrary assumption that a saturation effect takes place and can be represented by a constant QF at high LET values. It should be noted that under all circumstances the QF of 20 is applied to the dose from the heavy evaporation particles and recoil nuclei in calculating the rem dose since their LET is generally above 1750 MeV/cm.

Because of the uncertainties connected with the QF vs LET curve, H. J. Schaefer[3] suggested that the dose data be recorded in energy intervals in a manner similar to that described above so that any preferred set of QF conversion factors could be employed to calculate the rem dose with relative ease.

III. COMPARISON WITH OTHER WORK

In an attempt to establish the degree of reliability of the calculations, the results were compared with those obtained by other investigators, with particular interest taken in a comparison with two neutron dose experiments. Both experiments were performed with a spectrum of neutrons, and

doses calculated for our assumed infinite slab of tissue were applied as nearly as possible.

Shalnov[4] measured the dose as a function of depth in water and paraffin dummies due to neutrons which were incident in a broad beam and which resulted from the stripping reaction of 280-MeV deuterons on a thick copper target and also from the charge exchange of 480-MeV protons on beryllium. Serber[17] gives the energy spectrum of neutrons stripped from deuterons as

$$N(E)dE = \frac{\epsilon_d E_d}{\pi \left[(E - \frac{1}{2}E_d)^2 + \epsilon_d E_d \right]} \, dE \quad ,$$

where

   $N(E)dE$ = the number of neutrons in the energy range dE about E,

   E = neutron energy in MeV,

   E_d = the kinetic energy of the deuteron in MeV,

   ϵ_d = the binding energy of the deuteron = 2.18 MeV.

This is a spectrum with a peak at $\frac{1}{2}E_d$ and a full width at half maximum of $2 (E_d \epsilon_d)^{\frac{1}{2}}$. For 280-MeV deuterons these values are equal to 140 and 49 MeV, respectively.

The measured doses as a function of depth due to neutrons stripped from 280-MeV deuterons are compared in Fig. 4 with the calculated results for neutrons normally incident in a broad beam on an infinite slab of tissue. The results have not been normalized and agreement is seen to be good to a depth of 3 cm. At greater depths the calculated doses are higher than the measured doses, as might be expected since the calculation was performed for an infinite slab.
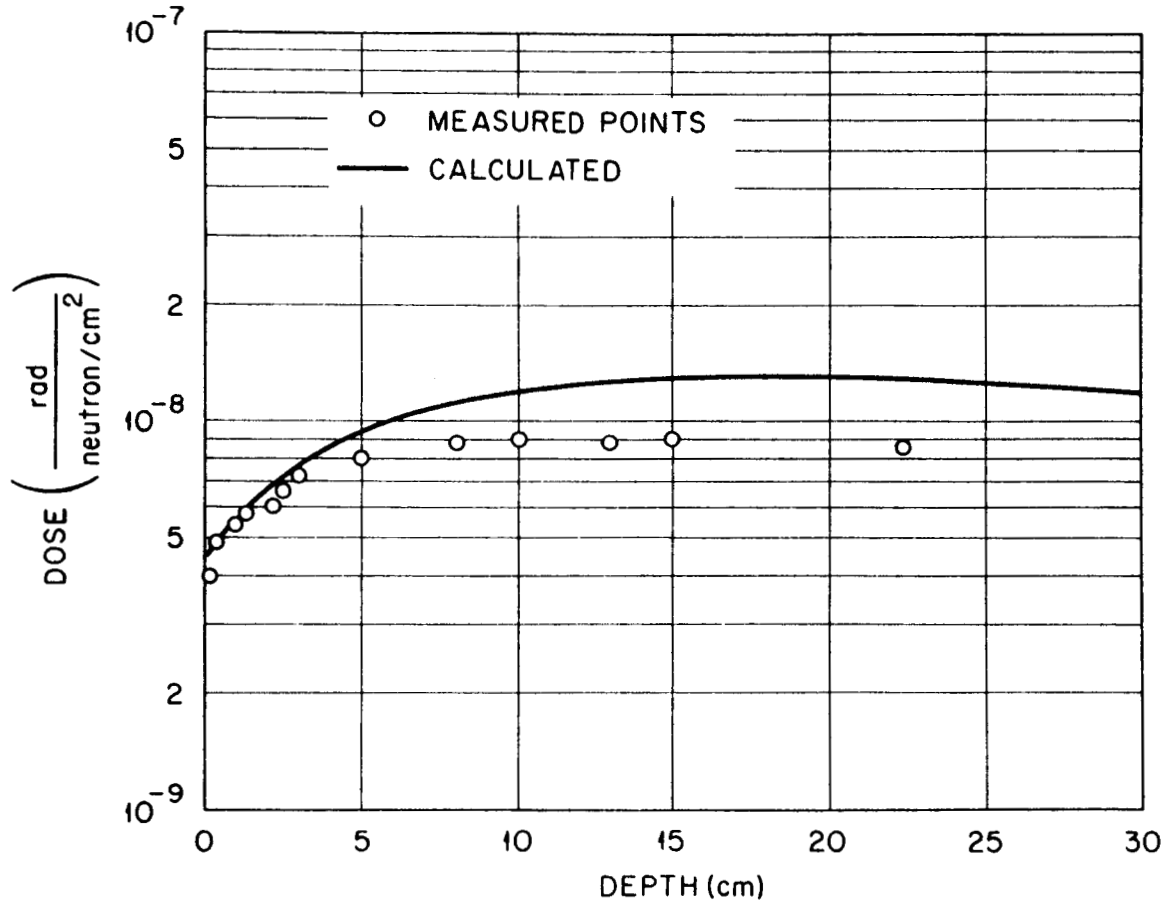
ORNL-DWG 64-10798

Fig. 4. Measured and Calculated Dose in Tissue vs Depth Due to Approx-imately 140-MeV Neutrons.

The neutron spectrum from the charge-exchange reaction of 480-MeV protons on beryllium as measured by Dzhelepov et al.[18] is given in Fig. 5, where the extrapolation assumed for this work is indicated. The average neutron energy is roughly 380 MeV, with 30% of the neutrons lying between 350 and 480 MeV, 25% between 250 and 350 MeV, and 21% between 150 and 250 MeV.

In an attempt to compare the calculated doses due to monoenergetic sources with the measured dose from the charge-exchange neutrons, the calculated doses for normal incidence were weighted rather crudely with the spectrum rather than calculating with the spectrum itself. The calculated doses for 400-MeV neutrons were weighted with the integral of the spectrum above 350 MeV. Similarly, the 300-MeV results were weighted with the integral from 250 to 350 MeV, the 200-MeV results with the integral from 150 to 250 MeV, and the 100-MeV doses with the integral below 150 MeV. The resultant weighted dose as a function of depth is compared in Fig. 6 with measured values for the charge-exchange neutrons. The experimental result in this case shows a flat behavior of the dose as a function of depth, whereas the calculated curve rises with increasing depth. It is interesting to note that the calculated dose vs depth curves for the 140-MeV neutron dose and the charge-exchange spectrum weighted dose agree generally in shape, rising with increasing depth due to the increase in secondaries. The experimental depth-dose curves for the stripped neutron and charge-exchange neutrons do not show this general shape agreement, possibly for the following reasons: As can be seen in Fig. 2,
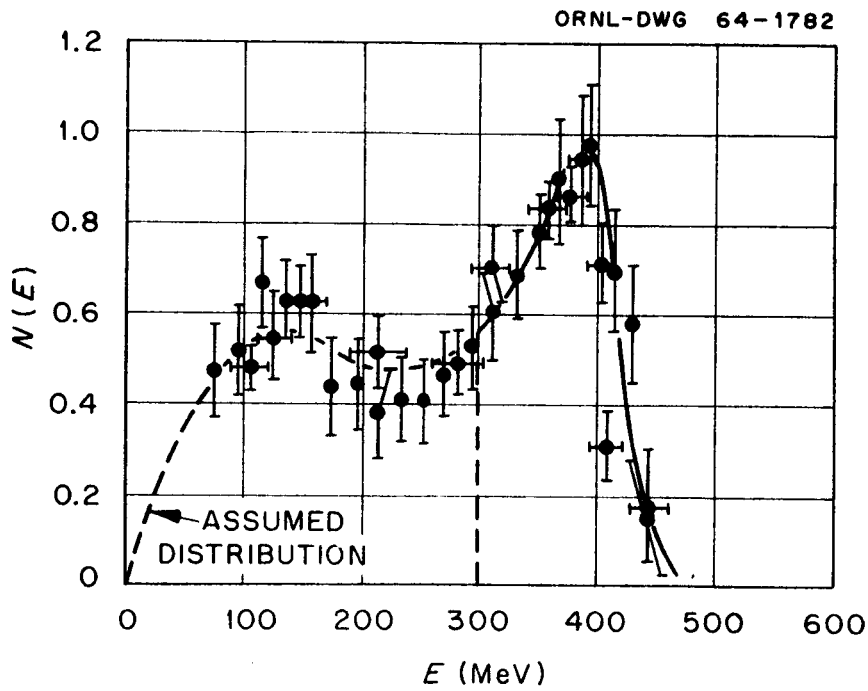
Fig. 5. Energy Spectrum of Neutrons Resulting from the Charge-Exchange of 480-MeV Protons on Beryllium.
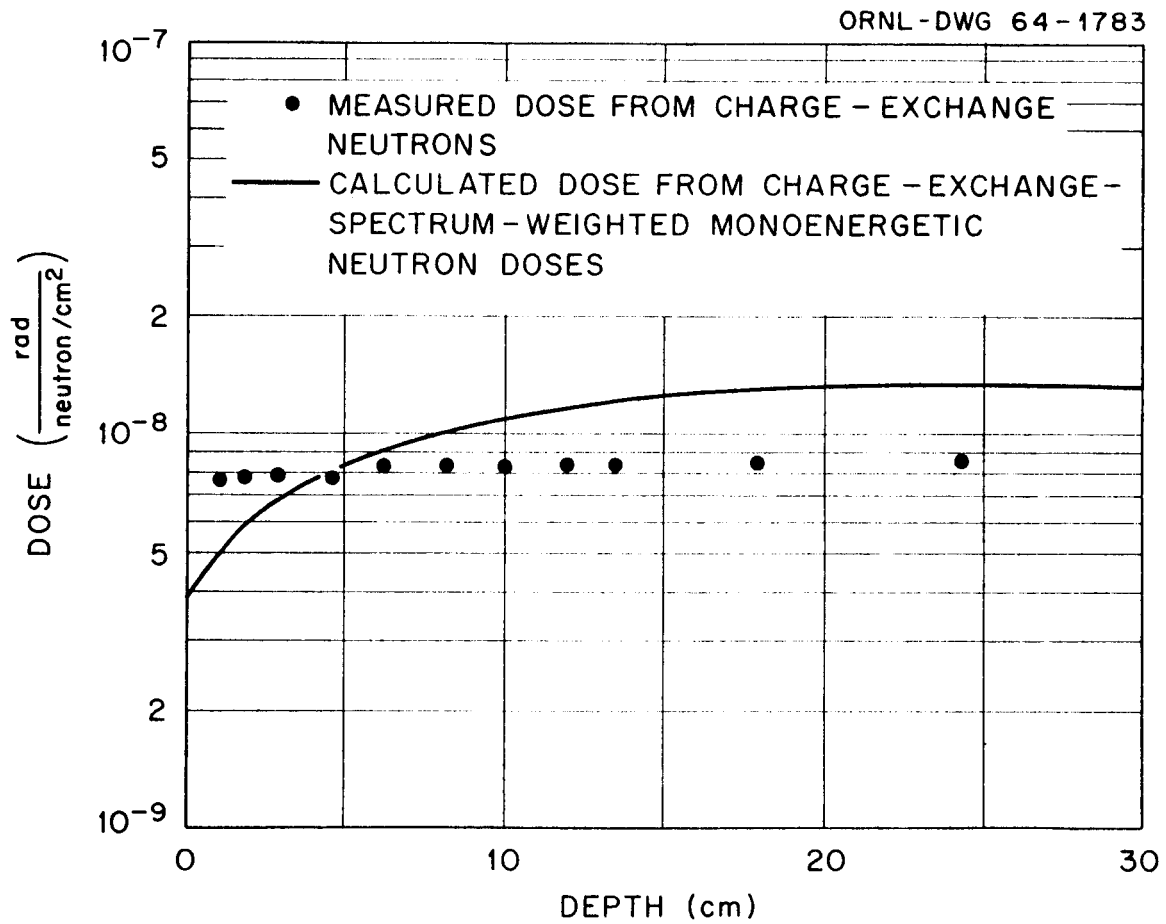
Fig. 6. Measured and Calculated Dose in Tissue vs Depth Due to Neutrons in a Charge-Exchange Spectrum of Mean Energy of 380 MeV.

the neutron cross sections rise rather steeply with decreasing energy below 100 MeV. Lower energy neutrons, then, impinging upon tissue will deposit relatively more energy at smaller depths than will higher energy neutrons, and the effect will be·to flatten the depth-dose curve or, for high enough cross sections, to cause the curve to decrease monotonically with increasing depth. Figure 7 illustrates the effect where calculated depth-dose curves for 200-, 60-, and 10-MeV monoenergetic normally incident neutrons are compared. If the charge-exchange spectrum were to rise so that half the neutrons appear below 80 MeV, or, alternatively, if a substantial background contribution were present at these lower energies, a crude calculation shows that the flat behavior of dose with depth would be accounted for.

Neary and Mulvey[1] have estimated the permissible currents of incident nucleons of energy in the range 40 to 1000 MeV which will produce a dose in a period of 40 hr equal to 0.3 rem, the value of maximum weekly dose recommended by the National Committee on Radiation Protection and Measurements.[19] They estimated the QF of the nucleons and assumed that all the energy was deposited within a distance equal to the range in the case of protons and within a mean free path in the case of neutrons. They then computed an average dose over these distances to arrive at the permissible incident current. Their results are compared in Fig. 8 with maximum currents based on the results of our calculations for both normally incident and isotropically incident nucleons. Our currents were determined by computing average-whole-body doses over the 30-cm slab for all the neutron calculations and for the protons of incident energy greater than 220 MeV, the energy at which the range of protons in tissue is 30 cm. For protons below 220 MeV the doses were averaged over the range of the protons.
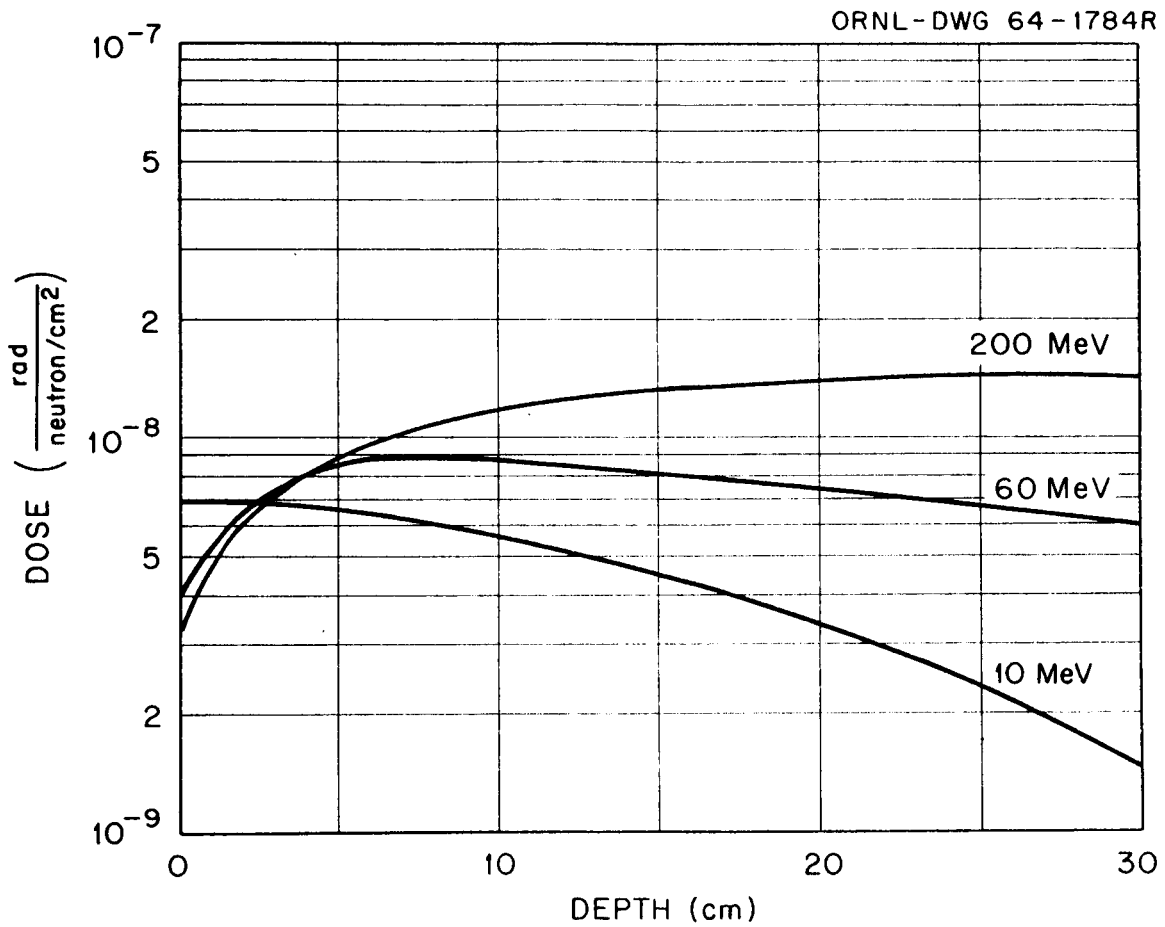
ORNL-DWG 64-1784R

Fig. 7. Comparison of the Calculated Dose vs Depth in Tissue for Normally Incident Monoenergetic 200-, 60-, and 10-MeV Neutrons.
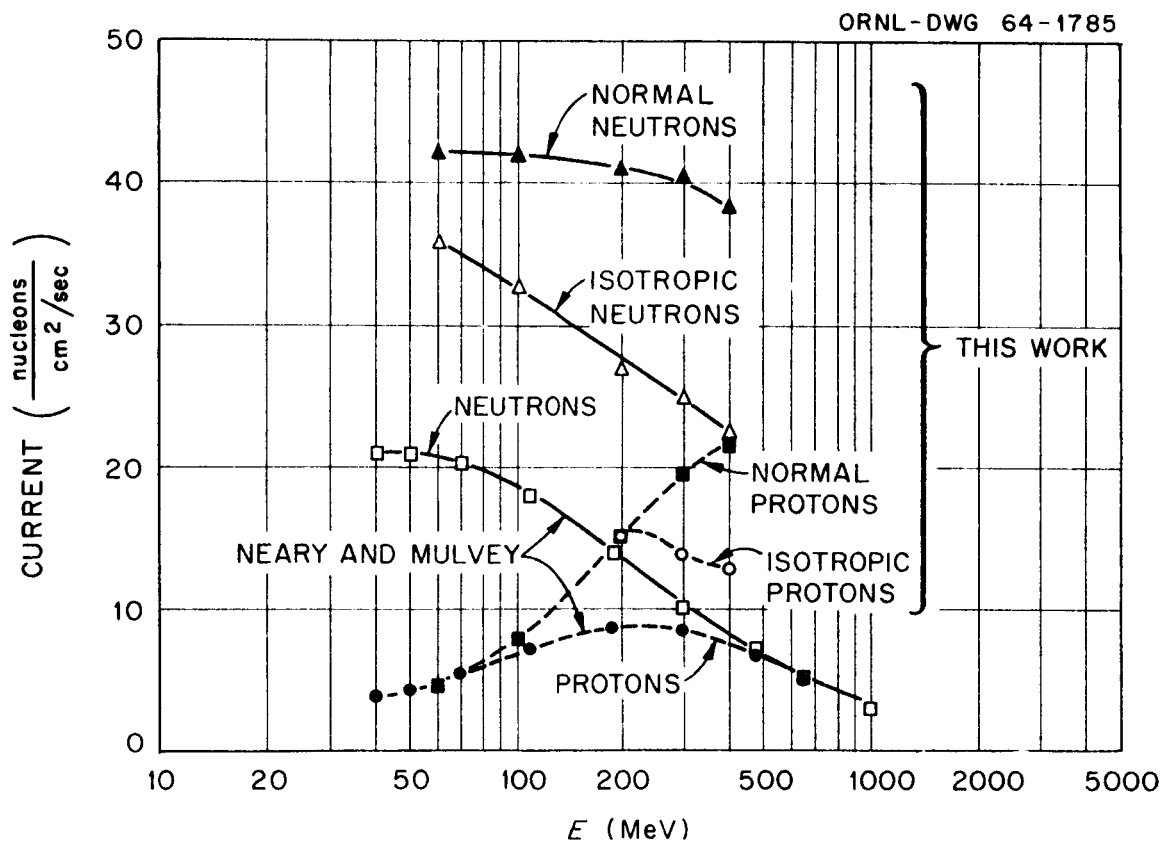
Fig. 8. Comparison of Fluxes of Nucleons to Produce a Dose of 0.3 Rem per 40 hr vs Incident Energy.

The differences are greatest in the case of neutrons, where our results in-
dicate that currents higher by a factor of 2 to 4 may be permitted. The
differences are chiefly due to Neary and Mulvey's assumption of complete
absorption of the neutron, whereas we considered a 30-cm-thick slab. The
mean free path for neutrons in the 100- to 400-MeV energy range is approx-
imately 80 cm, so that 70% of the primary neutrons at normal incidence pass
through the slab without suffering interaction and hence deposit no energy;
many of the secondary neutrons also escape. The permitted currents of
neutrons incident isotropically are, of course, less than those permitted
at normal incidence since the former neutrons travel, on the average,
twice as far as the latter in the slab.

The permitted proton currents resulting from our calculations are also
higher than those of Neary and Mulvey. At low energies the permitted cur-
rents agree but they start to diverge around 70 MeV, the divergence in-
creasing up to 220 MeV, the energy at which normally incident protons can
just get through the slab. This is due to our calculations giving
lower effective QF for the incident proton than that assumed by Neary and
Mulvey. Our effective QF, which is equal to the ratio of total rem to
total rad dose, falls from 1.3 at 100 MeV to 1.1 at 200 MeV (see Fig. 14
in Sect. IV), while the values of Neary and Mulvey rise from 1.24 at 70
MeV to 1.6 at 190 MeV. Above 220 MeV, our permitted current of normally
incident protons increases since the primaries are now able to escape,
as indicated in Fig. 14. The curve of permitted current for isotropically
incident protons, however, turns over above 220 MeV and falls, since the
higher energy protons produce more secondaries than do the lower energy
protons, and while the average rad dose remains constant with increasing
energy the rem dose increases slightly, as shown in Fig. 15 (see Sect. IV).

As a check on the calculation of the dose resulting from low-energy neutrons, the dose due to 10-MeV neutrons incident on a 30-cm-thick infinite slab of tissue in a broad beam was calculated and compared with a similar calculation by Snyder and Neufeld.[13] The calculated doses agreed when, as in Snyder and Neufeld's calculations, the inelastic scattering was treated as elastic scattering and the elastic-scattering angular distributions were assumed to be isotropic in the center-of-mass system of coordinates. It was observed, however, that when the elastic-scattering angular distribution was allowed to vary linearly with the cosine of the scattering angle in the center-of-mass system, the dose due to heavy recoil particles was reduced by a factor of about 2 (from 8.5×10^{-10} to 4.0×10^{-10} rad neutron^{-1} cm^{-2} at 5-cm depth) since forward scattering imparts less recoil energy to the target nuclei.

In view of this effect, the low-energy neutron doses should be recalculated, with both the anisotropy of elastic scattering and the inelastic scattering being taken into consideration.

IV. RESULTS

As stated previously, Monte Carlo calculations were performed for both normally and isotropically incident protons and neutrons with energies of 60, 100, 200, 300, and 400 MeV. Ten thousand source particles were used for each case. Partial results from the 200-MeV cases are presented in Figs. 9 through 12 to indicate typical results and the statistical uncertainties associated with the data. Additional details and the remainder of the cases are presented elsewhere.[5]

For the case of normal incidence the dose from primary protons presented in Fig. 9 approximates, as expected, the stopping-power curve for
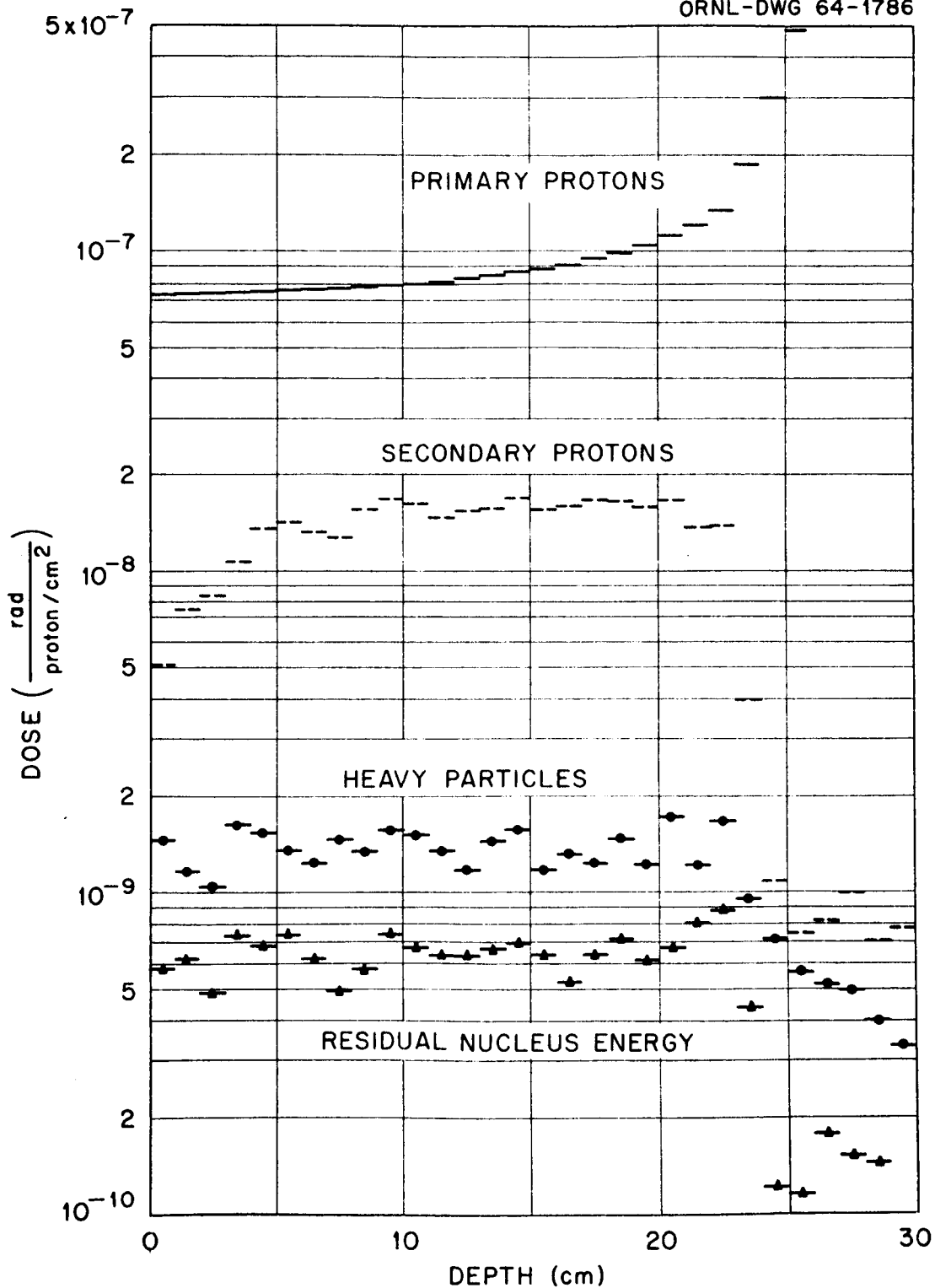
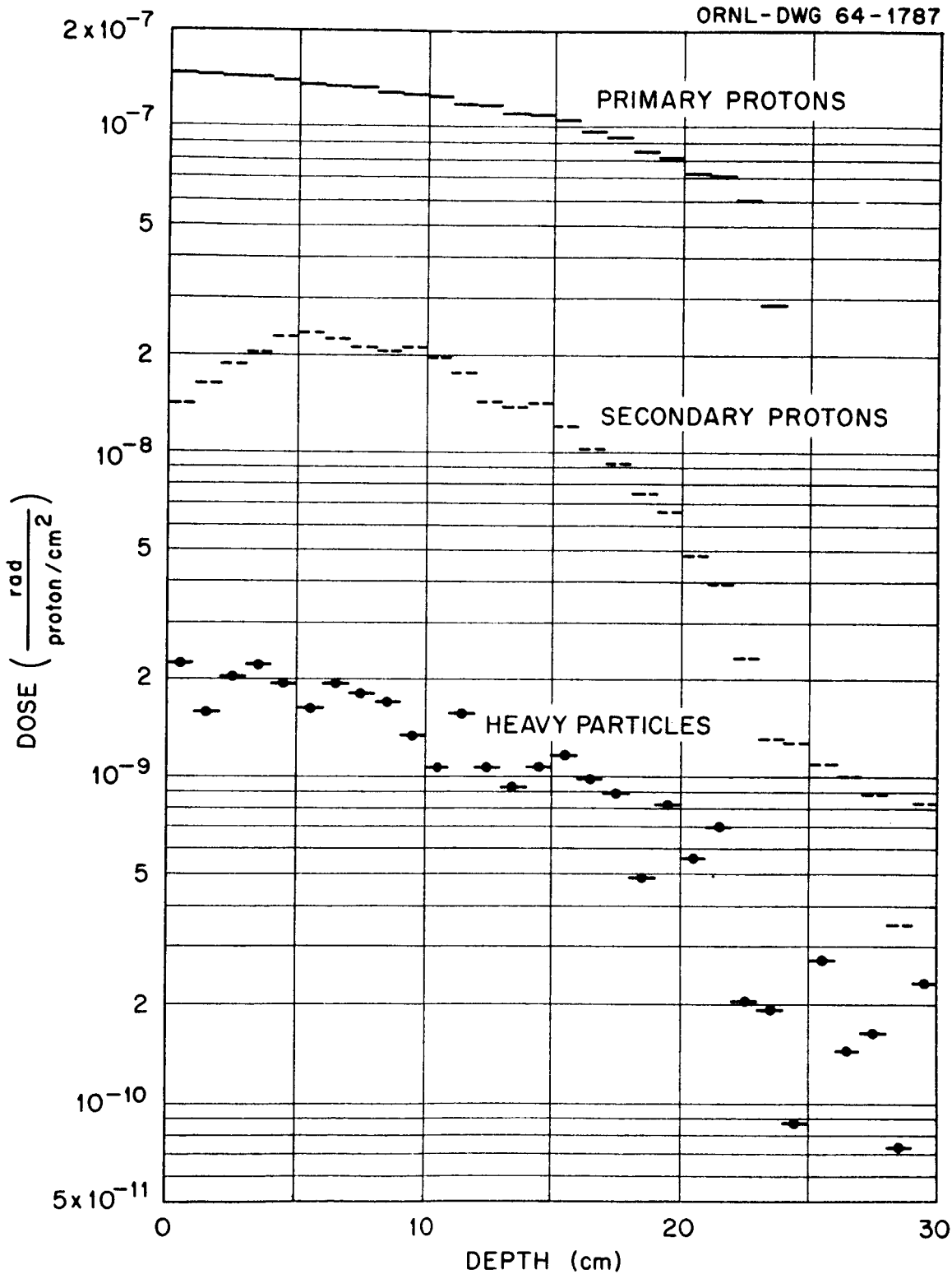Fig. 9. Dose vs Depth for 200-MeV Normally Incident Protons.

Fig. 10. Dose vs Depth for a Unit Current of 200-MeV Isotropically Incident Protons.
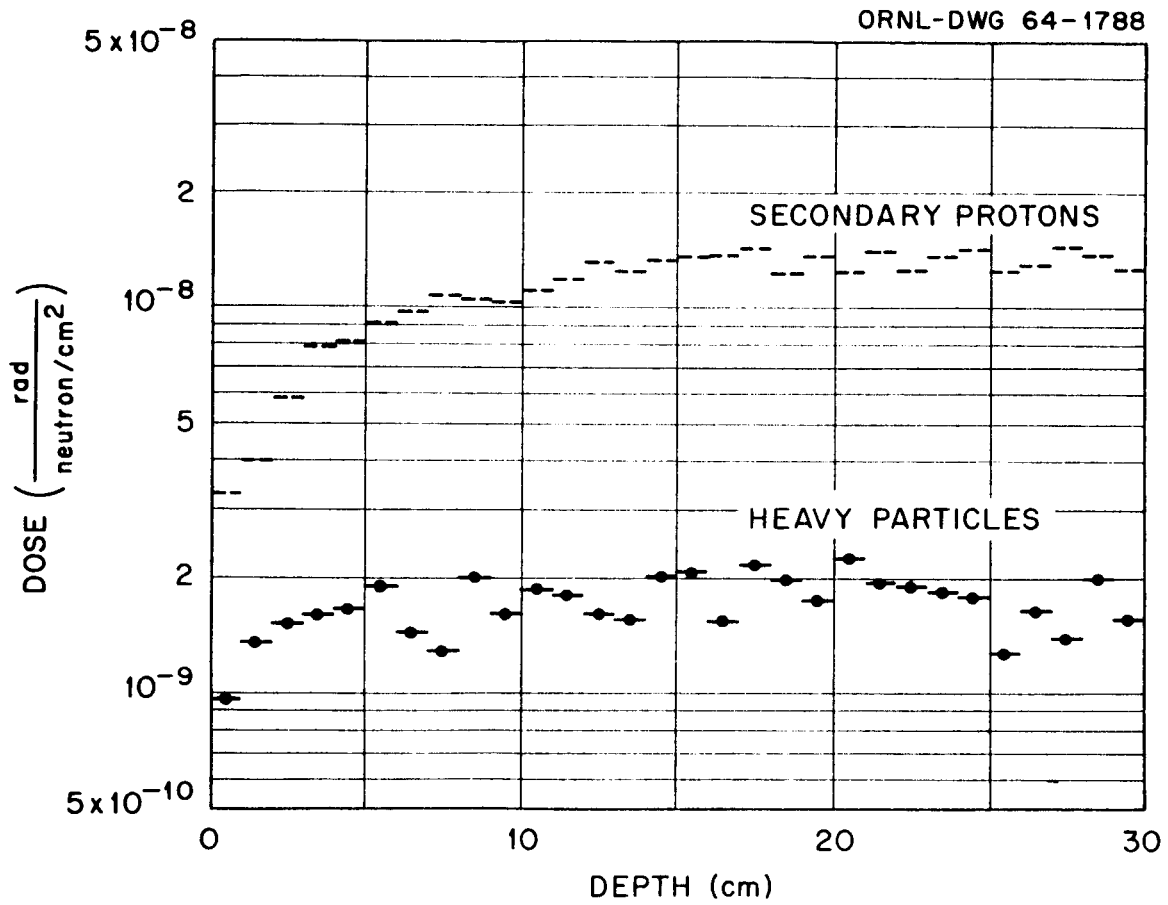
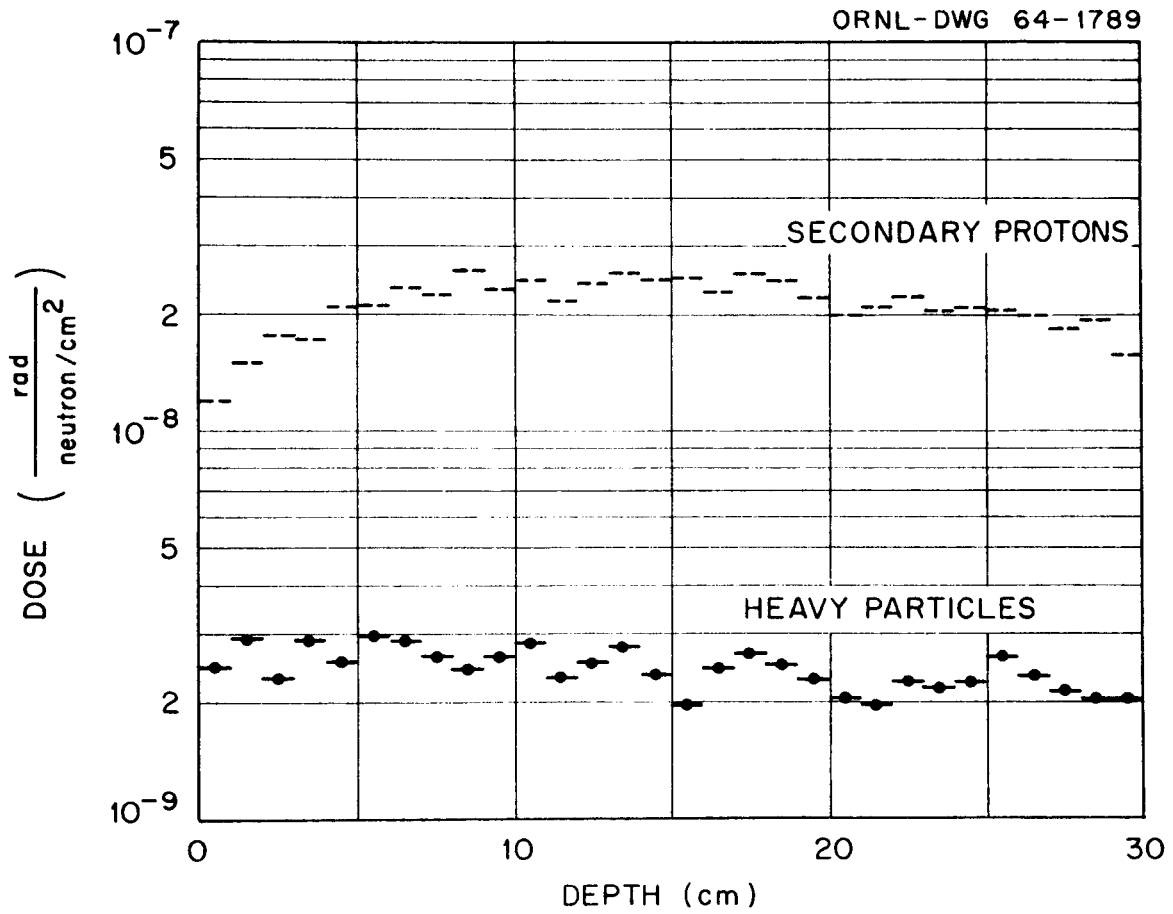Fig. 11. Dose vs Depth for 200-MeV Normally Incident Neutrons.

Fig. 12. Dose vs Depth for a Unit Current of 200-MeV Isotropically Incident Neutrons.

ionization energy loss as a function of depth in tissue. It is only an approximation because some of the protons are removed from the beam by nonelastic events, and so the energy deposition falls below the stopping-power curve. At 200-MeV incident energy the stopping power increases rapidly enough with decreasing energy (and hence with depth) to override the primary-beam depletion due to nonelastic events so that the dose increases with depth. At about 400 MeV the two effects almost balance and the energy deposition from the primary beam decreases slightly with depth, only to increase again near the end of the range as the stopping power increases. Of course, for normally incident 400-MeV protons the rise at the end of the range is not experienced in our model of the body because their range is 84 cm.

The energy deposition by secondary protons indicated in Fig. 9 includes the contribution from cascade protons ejected in nonelastic events, nuclear evaporation protons, and protons from elastic scattering with hydrogen whether they appeared as a result of neutron or proton interactions. Initially the dose from the secondary protons increases with depth as the number of secondary particles builds up from cascades initiated by the primary beam. Near the end of the range of the primary beam (26.5 cm) where the particle energies are low, the contribution from secondary protons decreases rapidly as a result of the decrease in the number of non-elastic events creating secondary particles. Beyond the range of the primary beam there is still a contribution from secondary protons ejected by neutrons that have migrated to that depth.

The dose from the heavy particles shown in Fig. 9 includes the con-tribution from the recoil of the residual nuclei after a nonelastic

event, nuclear recoils (other than protons) from elastic scattering of low-energy neutrons, and nuclear evaporation particles (other than protons). The dose from these particles is remarkably flat over most of the range of the primary beam. This is because it is roughly proportional to the collision density, since their energy is assumed to be deposited at the site of their birth. The dose decreases appreciably only near the end of the range where contributions come only from neutron-initiated events. The dose from residual nuclei shown in Fig. 9 actually indicates the energy created in the form of photons by transitions to the ground states of the residual nuclei after nonelastic events. The contribution to the dose from these radiations is usually so small for the cases considered that the migration of the photons has not been calculated; in fact, reference to the data is omitted in the remainder of the figures.

Figure 10 presents the results for the case of isotropically incident 200-MeV protons. The dose curves in this case are somewhat different from those for the case of normal incidence, as would be expected. First of all it is appropriate to note that the surface dose for the isotropic case for primary protons is higher by precisely a factor of 2 than the surface dose for normal incidence. This is strictly a result of normalizing both sets of data to a unit incident current of 1 particle per square centimeter of surface. For normal incidence the flux is equal to the current but for isotropic incidence it is exactly two times the current. Thus, since the energy deposition for the primary protons at the surface is proportional to the flux, the results for the isotropic case are greater by a factor of 2 than those for the normally incident case. Hence, it is important to keep the normalization in mind, and if comparisons are to be made on an equal flux basis, then the results of isotropic incidence should be divided by 2 in all cases.

The fact that the dose from the primary protons in Fig. 10 falls with depth is a consequence of the isotropy of the source and the finite range of the particles which combine with removal by nonelastic events to deplete the number of particles contributing to the dose as the depth increases. For the same reason the dose from secondary protons and heavy particles starts to decrease at smaller depths than in the normally incident case.

Figure 11 presents the data for normally incident 200-MeV neutrons. In this case, as in all cases with incident neutrons, contributions to the dose can come only from ionization energy loss by the secondary radiations. Thus only secondary-proton and heavy-particle contributions are indicated. Except for the region near and beyond the range of the primary proton beam, the two contributions are quite similar in shape and magnitude to the corresponding contributions from normally incident protons at the same source energy. This can be observed by comparing Fig. 11 with Fig. 9. At greater depths in the body the secondary contributions from the neutron source do not drop off because the neutrons do not have a finite range and on the average are not appreciably degraded in energy while passing through 30 cm of tissue.

For the case of isotropically incident neutrons shown in Fig. 12 it is possible to detect a decrease in the dose contribution of the secondaries beyond a 15-cm depth. This again is due to the geometric effects of the isotropic source coupled with the removal of the source particles by nonelastic events. To normalize the data to a unit flux, the results presented in Fig. 12 should be divided by 2. It should be noted that if the data for normal and isotropic incidence were normalized per unit flux, the dose from secondary particles could not be expected to be equal at the

surface although they might be approximately so. This is because, to a first approximation, the spatial distribution of the dose depends on the angular distribution of the emitted secondaries and the orientation of that angular distribution with the direction of the incoming particles. Since the secondary cascade protons are preferentially emitted in a forward direction, they cannot be expected to contribute significantly to the surface dose for normal incidence, whereas they can in the case of isotropic incidence because of the grazing angles of some of the incident particles. Hence, when the two sets of data are normalized on a unit flux basis, the contribution from secondary protons at the surface should be higher in the case of isotropic incidence.

From the detailed depth-dose data of all the cases calculated, certain doses were extracted to establish current-to-dose conversion factors. The particular ones chosen were the average whole-body dose, the surface dose, the dose at a depth of 5 cm, which is the average depth of the blood-forming organs, and the peak dose. These data are presented in Figs. 13 through 21. The detailed results for normally incident protons are presented in Fig. 13 as an indication of the significance of the various contributions. Here the primary proton, secondary proton, and heavy-particle rad and rem doses are presented separately.

In Fig. 13 the primary proton dose has a discontinuity at 215 MeV because above that energy the proton beam penetrates 30 cm of tissue and some of the energy is not deposited. An additional decrease in dose with increasing energy above 215 MeV is accounted for by the decrease in stopping power with increasing energy in this energy range. Thus less energy is deposited in the 30 cm of tissue as the energy increases. It is interesting to note that the rem dose of the primary or secondary protons in Fig. 13 is
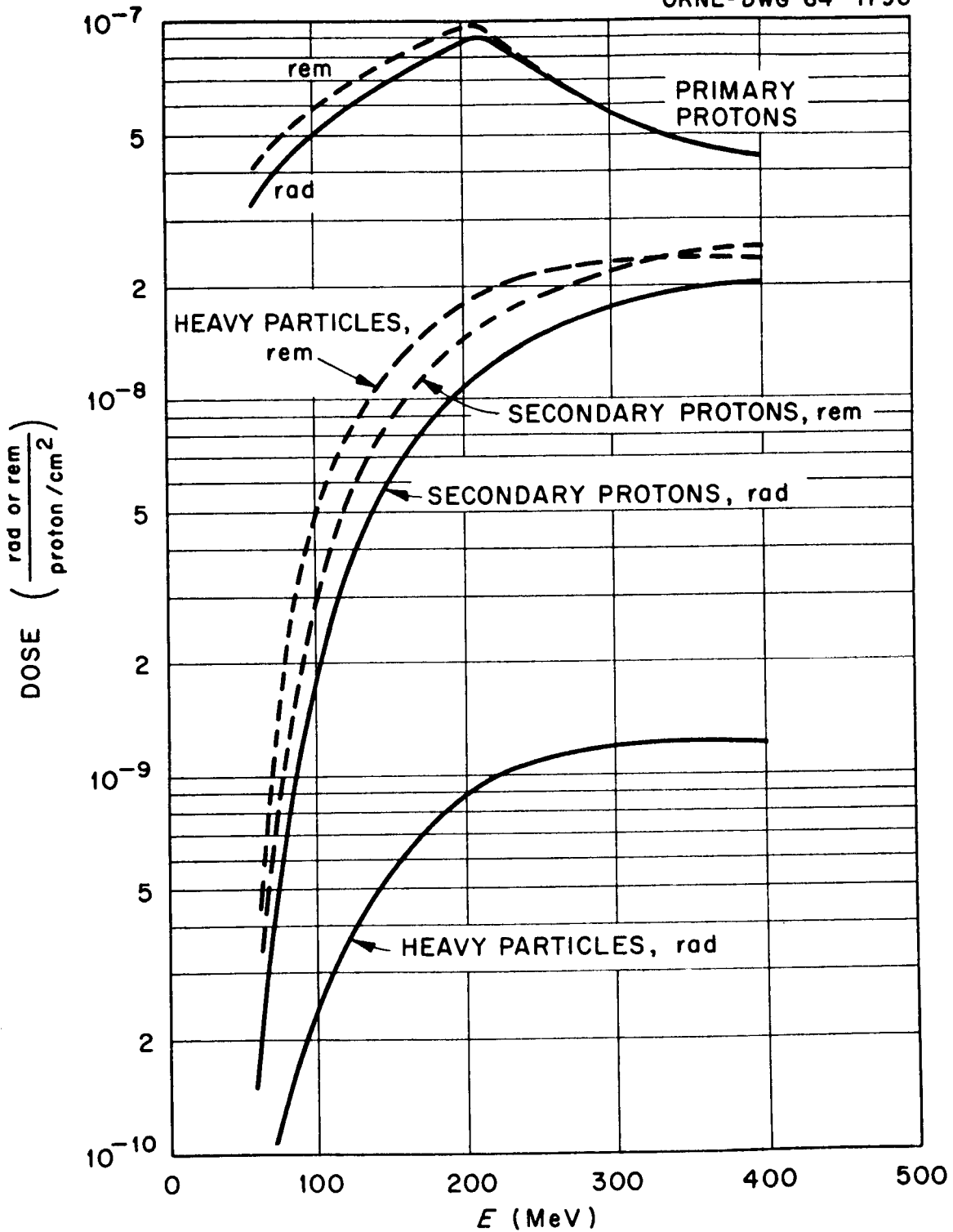
Fig. 13. Primary Proton, Secondary Proton, and Heavy-Particle Average Whole-Body Rad and Rem Doses Due to Normally Incident Protons as a Function of Incident Energy.
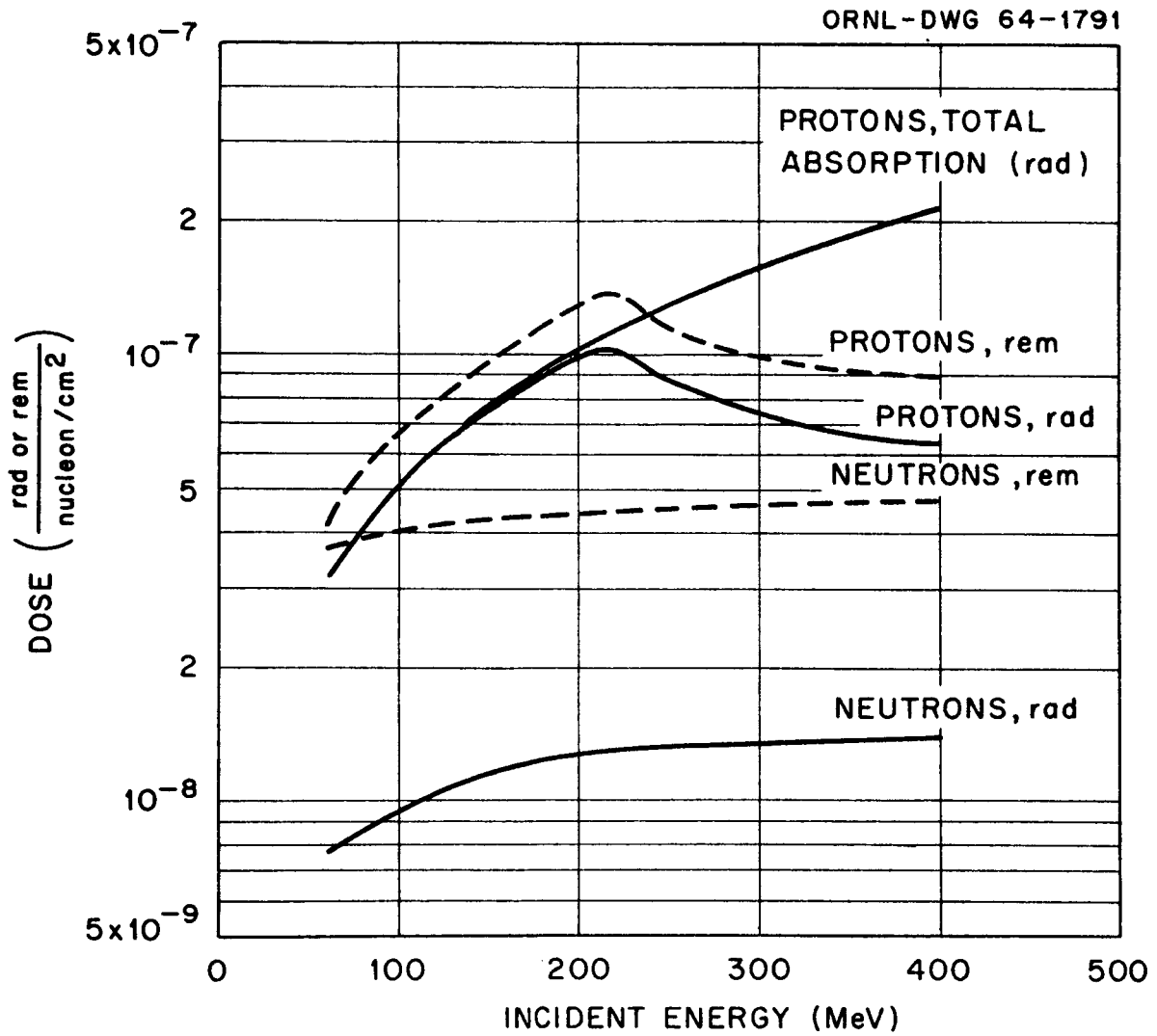
Fig. 14. Average Total Rad and Rem Doses vs Incident Energy for Normally Incident Protons and Neutrons.

Fig. 15. Average Total Rad and Rem Doses vs Incident Energy for a Unit Current of Isotropically Incident Protons and Neutrons.

Fig. 16. Total Dose at a Depth of 5 cm vs Incident Energy for Normally Incident Protons and Neutrons.

Fig. 17. Total Dose at a Depth of 5 cm vs Incident Energy for a Unit Current of Isotropically Incident Protons and Neutrons.

Fig. 18. Total Dose at the Surface vs Incident Energy for Normally Incident Protons and Neutrons.

Fig. 19. Total Dose at the Surface vs Incident Energy for a Unit Current of Isotropically Incident Protons and Neutrons.

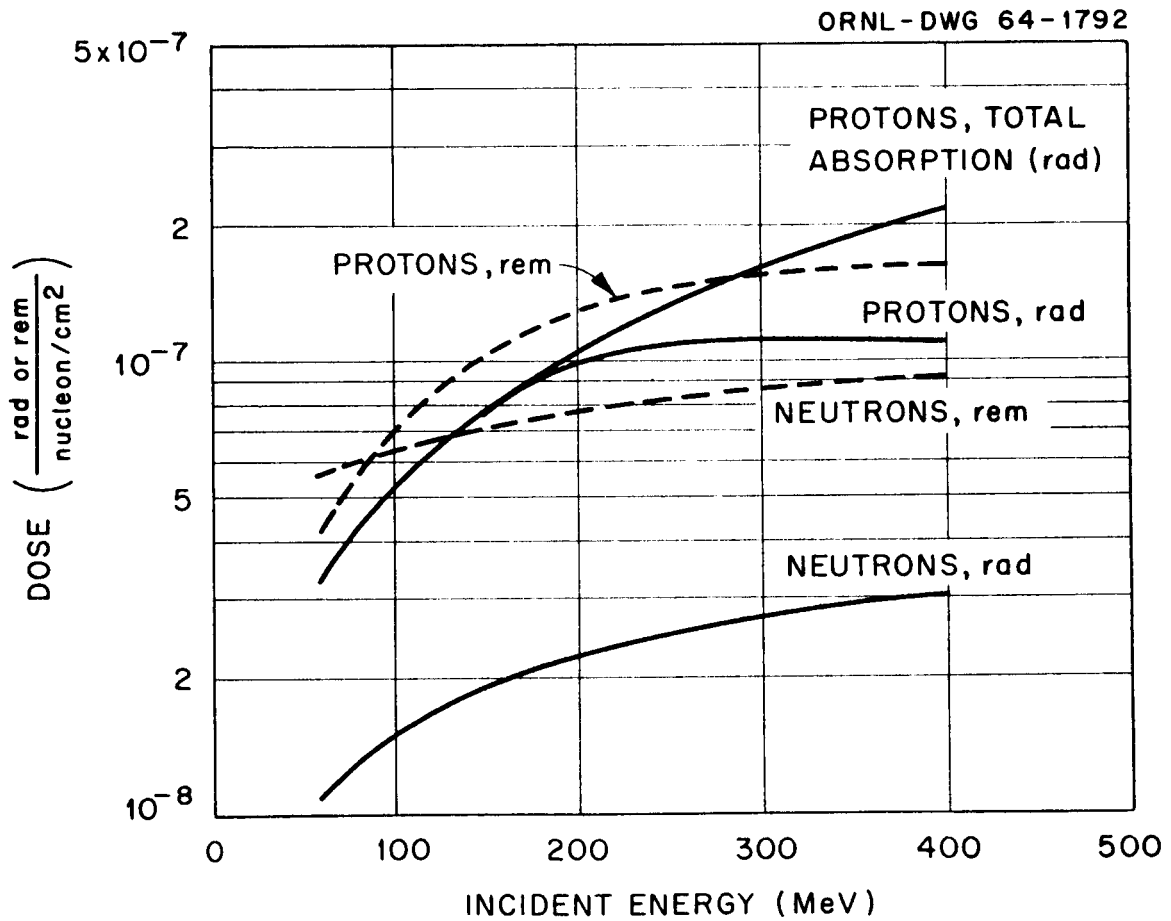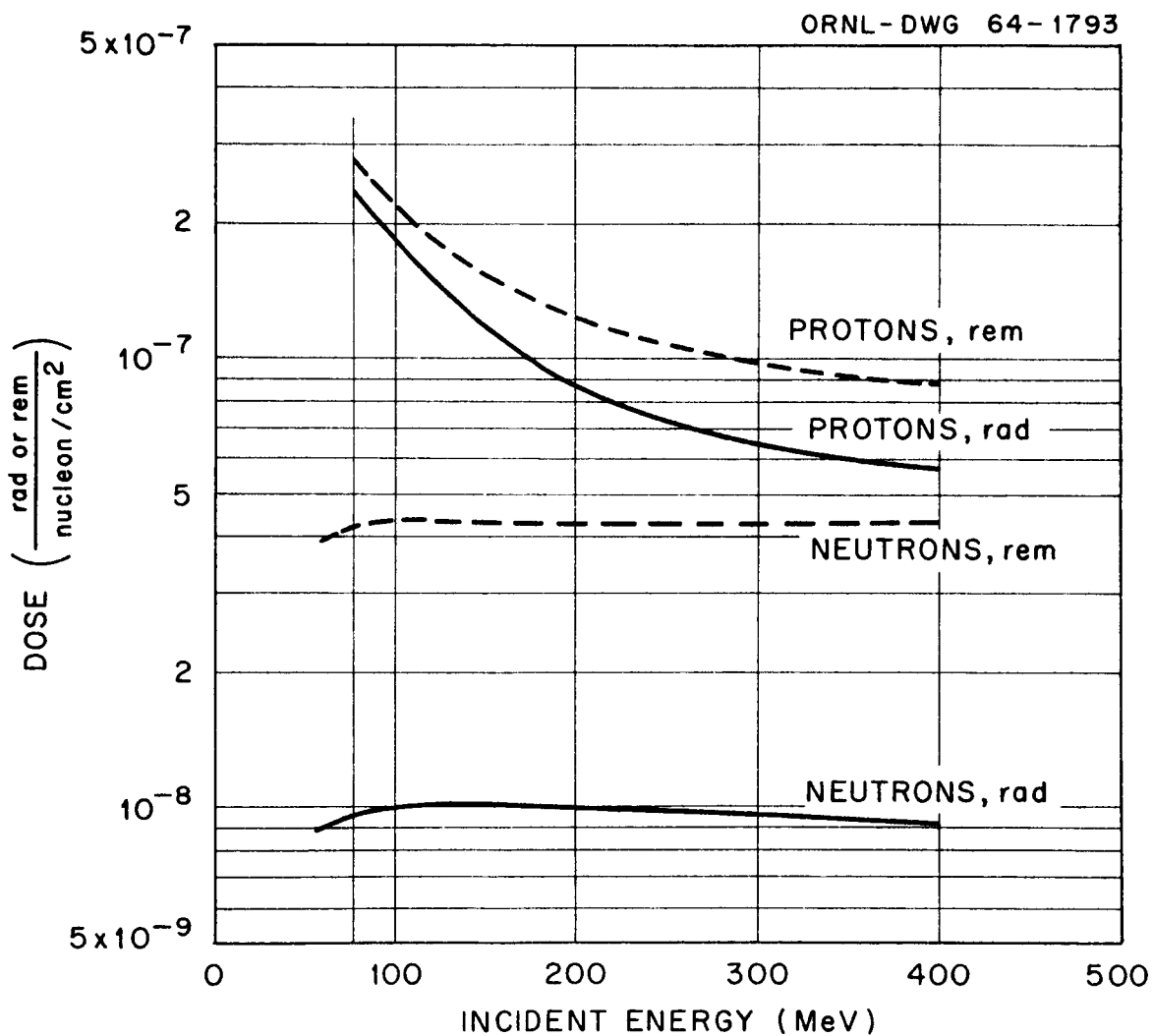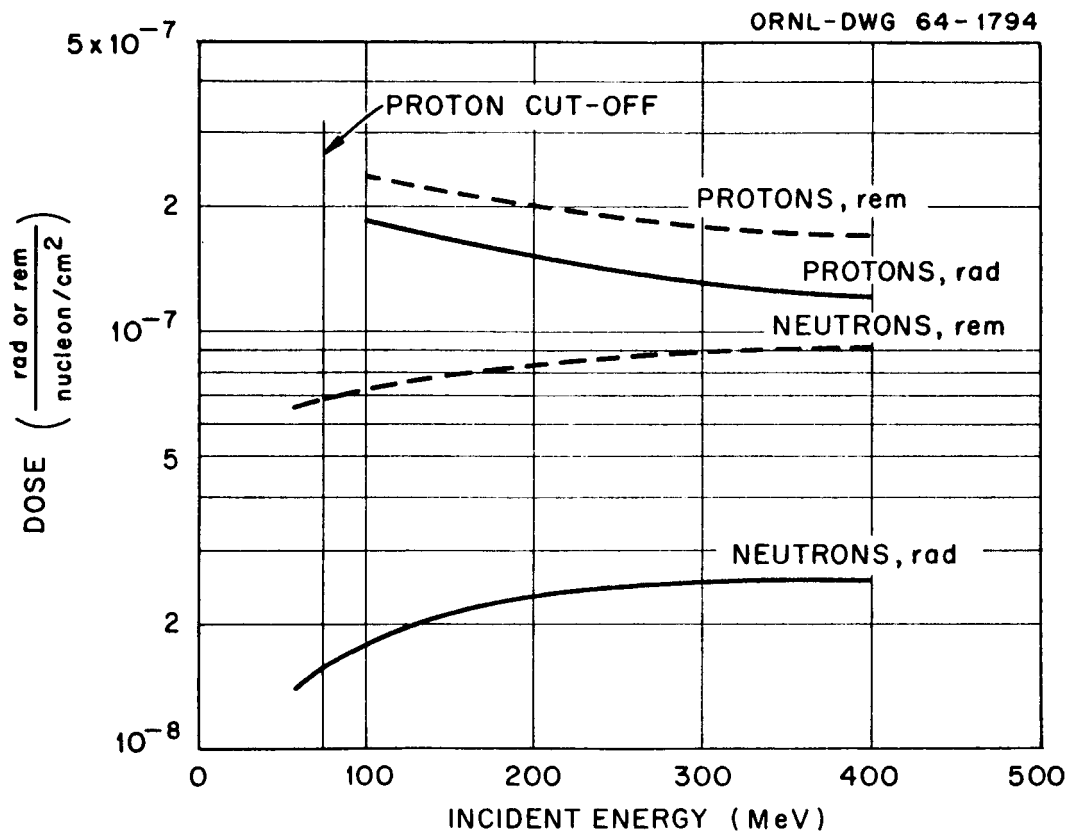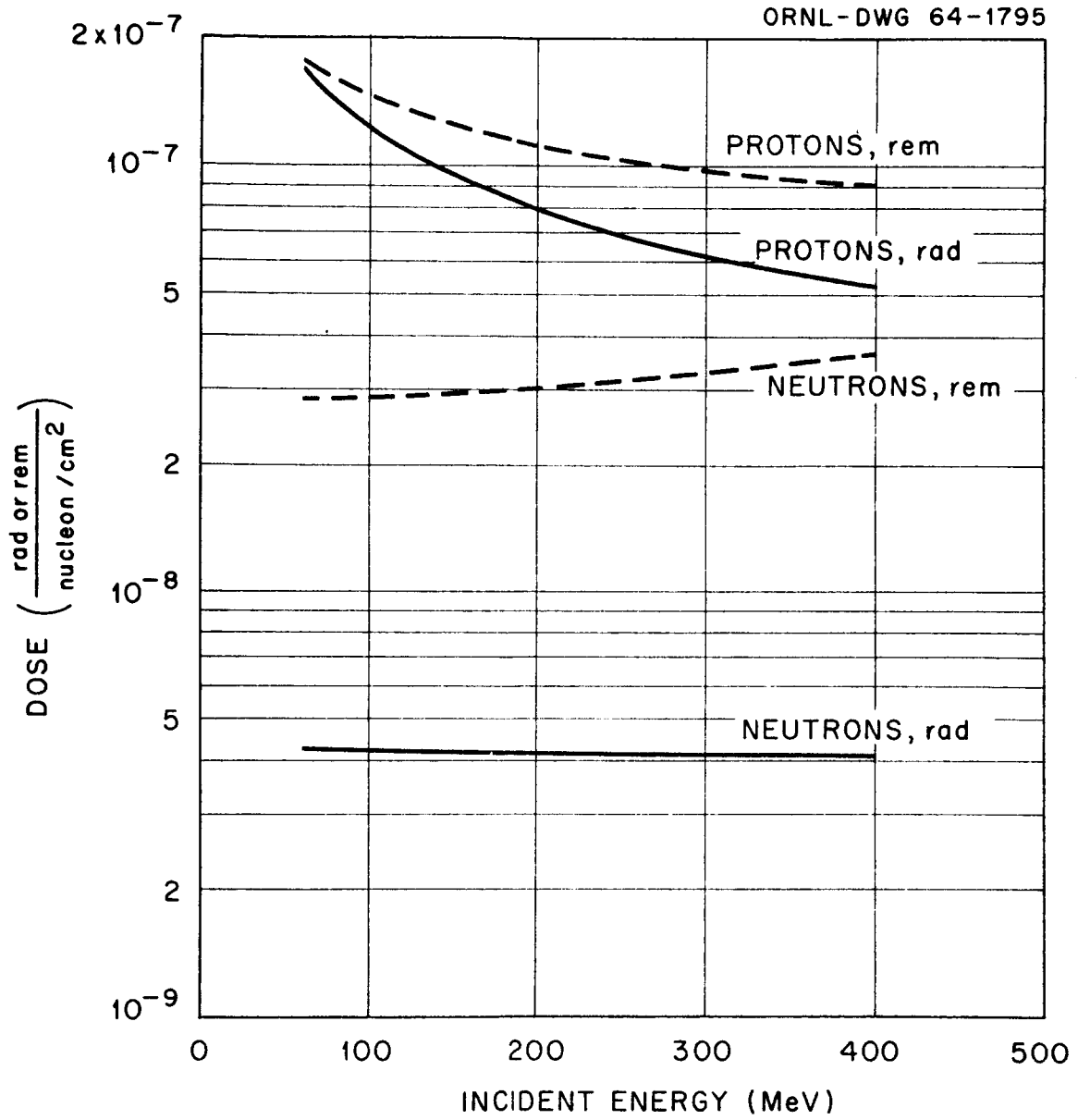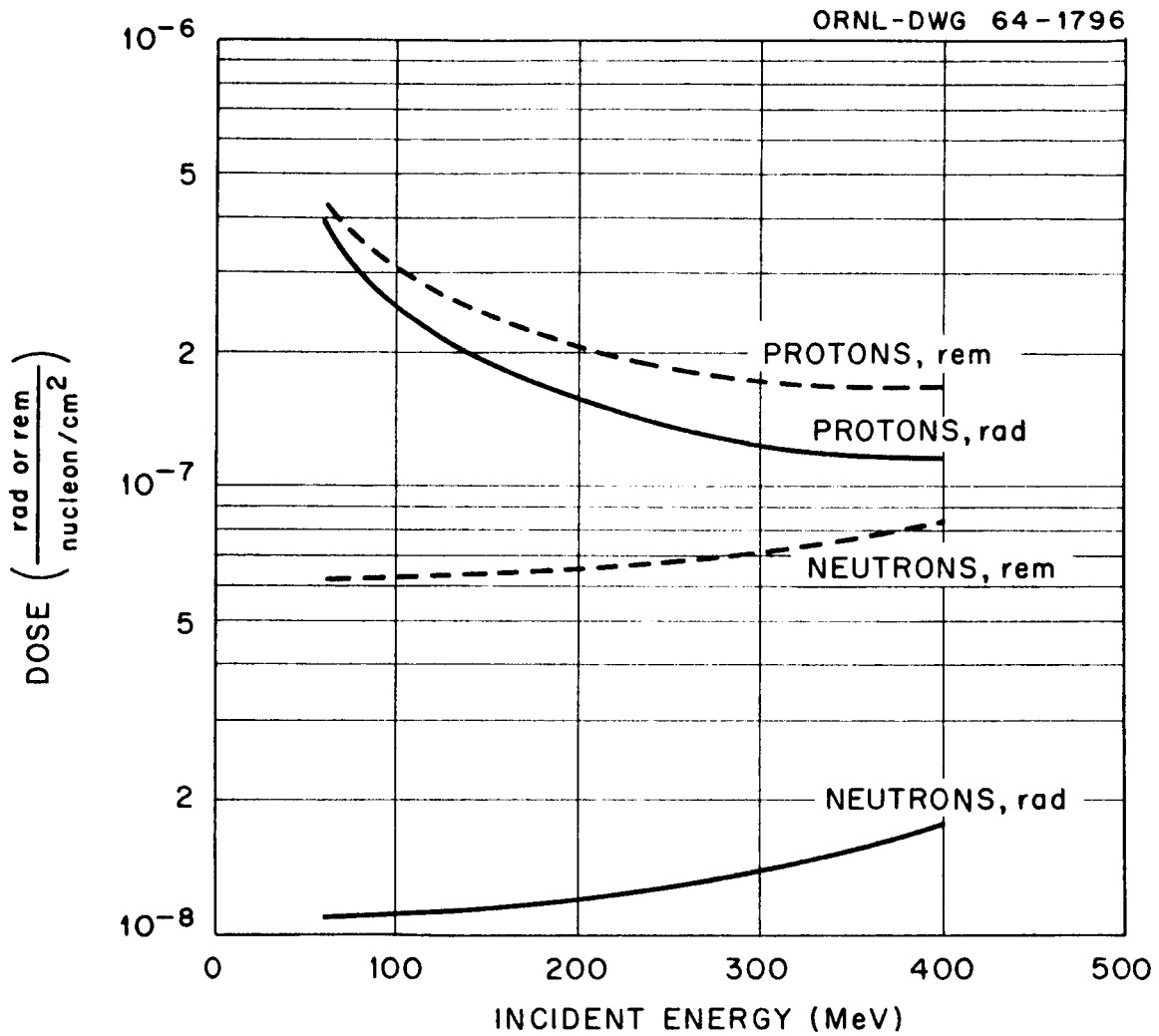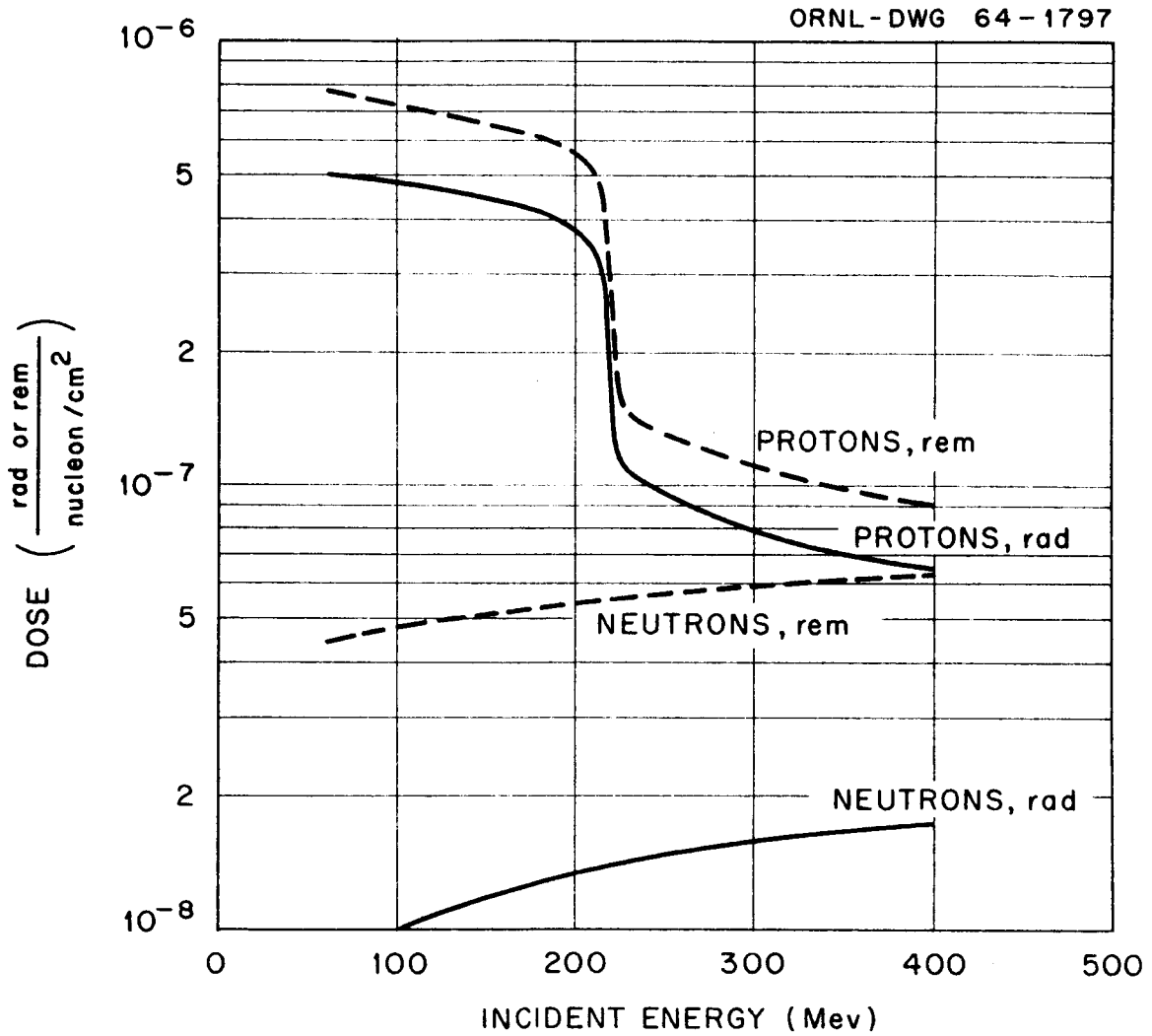Fig. 20. Maximum Total Dose vs Incident Energy for Normally Incident Protons and Neutrons.
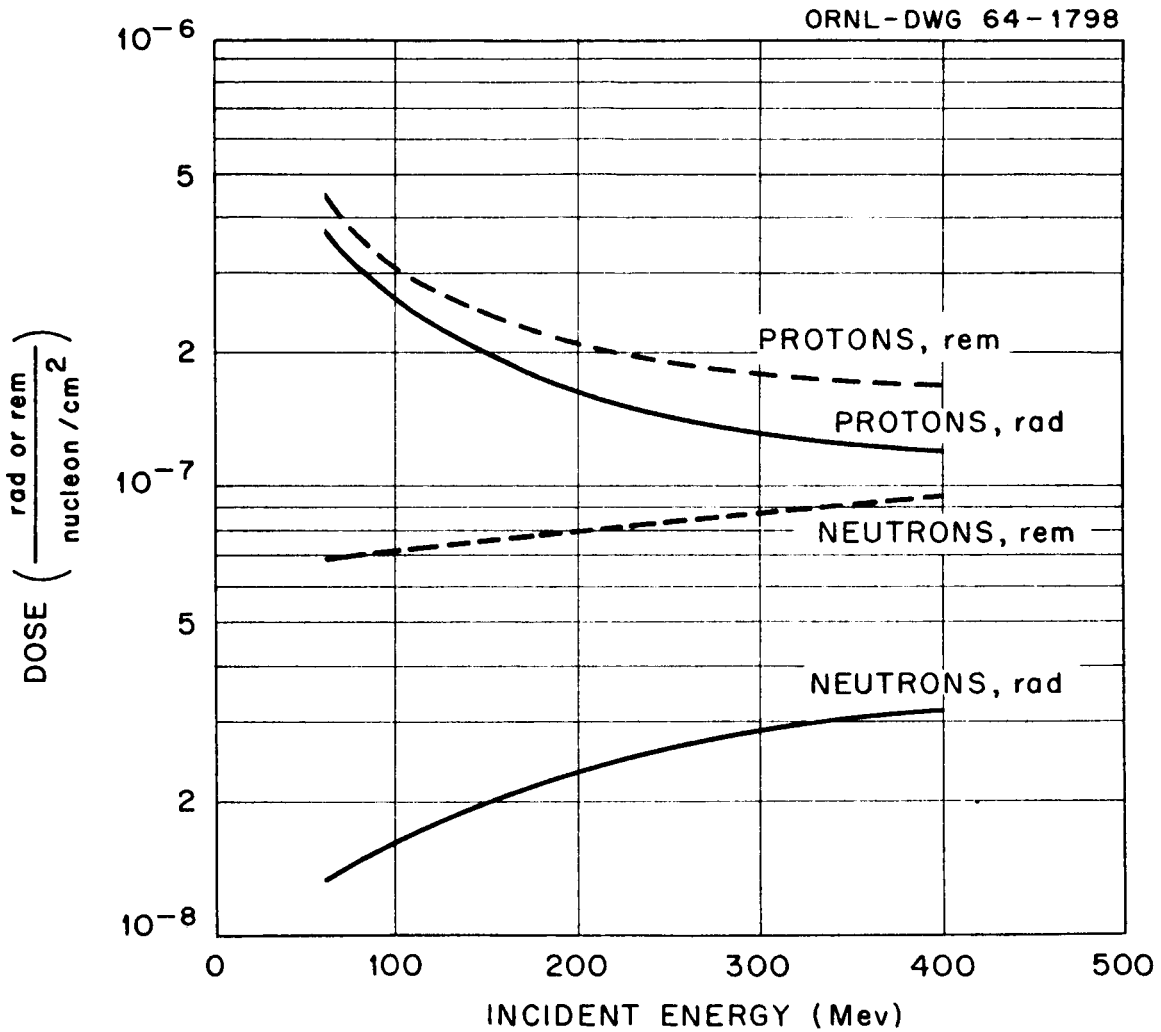
ORNL-DWG 64-1798

Fig. 21. Maximum Total Dose vs Incident Energy for a Unit Current of Isotropically Incident Protons and Neutrons.

not appreciably different from the corresponding rad doses. This is because most of the protons are created with energies well above 1 MeV and they therefore deposit the greatest fraction of their energy while the associated QF is close to unity. On the other hand, the rem dose of the heavy particles is exactly a factor of 20 above the rad dose because the LET of these particles is always above 1750 MeV/cm. This interesting situation, which admittedly depends on the ad hoc but perhaps reasonable assumption that the QF is 20 and constant at high-LET values, causes the heavy-particle contribution to the total rem dose to be greater than the secondary proton dose for most energies. For instance, at 100 MeV the secondary proton rem dose is approximately 6% of the total, while the heavy-particle rem dose contributes 10%. At 400 MeV these contributions are each approximately 35%.

Figure 14 presents the results for the average whole-body rad and rem doses for both normally incident neutrons and protons. Also shown is the average whole-body rad dose that would be received if the proton beam were totally absorbed. In comparison with the latter curve, it is easy to see that below 215 MeV little error would be introduced if the whole-body rad dose were calculated as if all the energy were totally absorbed.

The average QF is obtained by dividing the rem dose by the rad dose. In all cases presented this average QF is significantly greater for incident neutrons than for incident protons, the reason being that in the case of incident protons the dose from the primary protons with its associated QF, which is near unity, makes the most significant contribution to the total rad or rem dose. Thus the average QF would be expected to be close to unity. In the case of incident neutrons approximately 11% of the rad dose is contributed by the heavy particles, but its associated QF of 20 makes it the most significant contributor to the rem dose

(the QF associated with the secondary proton dose is close to unity).
An approximate calculation indicates that under these circumstances the
average QF should be close to 3 for the neutron cases. Indeed, the average
QF for normally incident protons ranges from 1.3 at 100 MeV to 1.4 at 400
MeV, while for normally incident neutrons it ranges from 4.2 at 100 MeV
to 3.4 at 400 MeV.

The curves for the average whole-body dose for isotropically incident
particles shown in Fig. 15 are quite similar to the corresponding ones from
the normally incident cases, and little need be said about them.

In Figs. 16 and 17, where the doses at a depth of 5 cm are reported,
there is a definite cutoff at 80 MeV for incident protons. This is because
the range of protons of approximately 80 MeV and below is less than 5 cm in
tissue and cannot make a contribution at that depth.

The curves for the surface doses shown in Figs. 18 and 19 are not
markedly different from the corresponding 5-cm-depth dose curves.

Figures 20 and 21 present the maximum dose curves for normally incident
and isotropically incident neutrons and protons. The depths at which these
maxima occur are presented in Table 2. The apparent discontinuity in the

Table 2
Depth at Which Maximum Dose Occurs

Source	Depth (cm) for Energies of				
	400 MeV	300 MeV	200 MeV	100 MeV	60 MeV
Normally incident protons	30	30	24-25	6-7	
Normally incident neutrons	30	30	20-30	5-10	5
Isotropically incident protons	5	5	5	3	0
Isotropically incident neutrons	15-25	15-25	15	5-10	0

normally incident proton curve shown in Fig. 20 is explained by the fact that below 215-MeV incident energy the maximum occurs at the end of the range of the protons where the stopping power is very high. Above 215-MeV incident energy the range of protons is greater than 30 cm; so the maximum in the body occurs at some intermediate proton energy where the stopping power is much less than at the end of its range. The maximum doses for energies below 215 MeV were obtained by averaging the dose over the last centimeter of its range.

The current-to-rem-dose conversion curves shown in Figs. 14 through 21 can be fitted by an expression of the form

$$\log_{10} D = A + BE + CE^2 \quad ,$$

where D is the dose in rem per nucleon per cm^2 and E is the energy in MeV. Tables 3 and 4 contain the values of the coefficients for normally and isotropically incident protons and neutrons, respectively.

Tables 5 through 8 present the breakdown of the energy deposition data for the cases in which the current-to-dose factors were calculated. With these data and a preferred or updated set of QF's, it will be relatively easy to construct a revised set of current-to-rem-dose conversion factors. Data from which conversion factors for any other depth or condition can be obtained are contained in another report.[5]

In most cases the data presented in Tables 5 through 8 came directly from the output of the computer routine. However, some of the data resulted from extrapolation or interpolation as required when the data deviated significantly from the apparent trend. In the case of low-energy protons a deviation often occurred when the range of the particle ended in a particular 1-cm-depth interval, in which case the averaging was not done

Table 3. Coefficients of the Expansion for the Rem Dose for Normally and Isotropically Incident Protons

Dose and Energy Range	Normally Incident Protons			Isotropically Incident Protons		
	A	B	C	A	B	C
Average whole body						
at 60–215 MeV	-7.72	6.4×10^{-3}	-1.12×10^{-5}	-7.79	7.88×10^{-3}	-1.7×10^{-5}
at 215–400 MeV	-6.20	-4.32×10^{-3}	5.5×10^{-6}	-7.07	1.22×10^{-3}	-1.34×10^{-6}
5 cm deep						
at 80–400 MeV	-6.27	-4.56×10^{-3}	6.43×10^{-6}	-6.57	-5.43×10^{-4}	0
Surface						
at 60–400 MeV	-6.64	-2.17×10^{-3}	2.86×10^{-6}	-6.30	-2.66×10^{-3}	3.68×10^{-6}
Maximum						
at 60–215 MeV	-6.02	-1.2×10^{-3}	0	-6.26	-2.92×10^{-3}	4.1×10^{-6}
at 215–400 MeV	-6.62	-1.12×10^{-3}	0			

Table 4. Coefficients of the Expansion for the Rem Dose for Normally and Isotropically Incident Neutrons at 60–400 MeV

Dose	Normally Incident Neutrons			Isotropically Incident Neutrons		
	A	B	C	A	B	C
Average whole body	-7.43	2.67×10^{-4}	0	-7.26	5.64×10^{-4}	0
5 cm deep	-7.38	0	0	-7.18	3.92×10^{-4}	0
Surface	-7.59	3.68×10^{-4}	0	-7.26	4.47×10^{-4}	0
Maximum	-7.35	3.83×10^{-4}	0	-7.18	4.0×10^{-4}	0

Table 5. Average Whole-Body Dose

Source	Incident Energy (MeV)	Dose (rads per nucleon/cm^2)						
		Protons at					Heavy Particles	Total
		0-1 MeV	1-5 MeV	5-10 MeV	10-50 MeV	>50 MeV		
Normally incident protons	400	3.9×10^{-10}	1.2×10^{-9}	1.1×10^{-9}	5.2×10^{-9}	5.6×10^{-8}	1.2×10^{-9}	6.5×10^{-8}
	300	3.9×10^{-10}	1.3×10^{-9}	1.1×10^{-9}	5.0×10^{-9}	6.4×10^{-8}	1.2×10^{-9}	7.3×10^{-8}
	200	7.7×10^{-10}	2.8×10^{-9}	3.0×10^{-9}	2.0×10^{-8}	7.2×10^{-8}	1.0×10^{-9}	1.0×10^{-7}
	100	5.9×10^{-10}	2.3×10^{-9}	2.7×10^{-9}	2.1×10^{-8}	2.6×10^{-8}	2.5×10^{-10}	5.3×10^{-8}
	60	5.4×10^{-10}	2.1×10^{-9}	2.7×10^{-9}	2.1×10^{-8}	5.3×10^{-9}	2.2×10^{-11}	3.2×10^{-8}
Normally incident neutrons	400	3.8×10^{-10}	1.2×10^{-9}	9.7×10^{-10}	3.7×10^{-9}	6.4×10^{-9}	1.5×10^{-9}	1.4×10^{-8}
	300	3.5×10^{-10}	1.1×10^{-9}	9.4×10^{-10}	3.7×10^{-9}	5.7×10^{-9}	1.4×10^{-9}	1.3×10^{-8}
	200	3.7×10^{-10}	1.1×10^{-9}	9.7×10^{-10}	4.0×10^{-9}	4.8×10^{-9}	1.4×10^{-9}	1.3×10^{-8}
	100	3.9×10^{-10}	1.2×10^{-9}	1.0×10^{-9}	3.9×10^{-9}	1.6×10^{-9}	1.4×10^{-9}	9.5×10^{-9}
	60	4.0×10^{-10}	1.2×10^{-9}	1.1×10^{-9}	3.6×10^{-9}	1.4×10^{-10}	1.2×10^{-9}	7.6×10^{-9}
Isotropically incident protons	400	6.9×10^{-10}	2.5×10^{-9}	2.1×10^{-9}	1.0×10^{-8}	9.2×10^{-8}	2.0×10^{-9}	1.1×10^{-7}
	300	6.9×10^{-10}	2.3×10^{-9}	2.2×10^{-9}	1.2×10^{-8}	9.3×10^{-8}	1.6×10^{-9}	1.1×10^{-7}
	200	7.8×10^{-10}	2.8×10^{-9}	3.1×10^{-9}	2.1×10^{-8}	7.2×10^{-8}	1.0×10^{-9}	1.0×10^{-7}
	100	5.9×10^{-10}	2.3×10^{-9}	2.7×10^{-9}	2.1×10^{-8}	2.6×10^{-8}	2.5×10^{-10}	5.3×10^{-8}
	60	5.4×10^{-10}	2.1×10^{-9}	2.7×10^{-9}	2.1×10^{-8}	5.5×10^{-9}	2.4×10^{-11}	5.2×10^{-8}
Isotropically incident neutrons	400	7.1×10^{-10}	2.2×10^{-9}	1.8×10^{-9}	7.7×10^{-9}	1.5×10^{-8}	2.6×10^{-9}	3.0×10^{-8}
	300	6.7×10^{-10}	2.1×10^{-9}	1.8×10^{-9}	7.3×10^{-9}	1.2×10^{-8}	2.5×10^{-9}	2.6×10^{-8}
	200	6.7×10^{-10}	2.1×10^{-9}	1.8×10^{-9}	7.4×10^{-9}	8.4×10^{-9}	2.4×10^{-9}	2.3×10^{-8}
	100	6.3×10^{-10}	2.0×10^{-9}	1.6×10^{-9}	6.4×10^{-9}	2.4×10^{-9}	2.1×10^{-9}	1.5×10^{-8}
	60	5.9×10^{-10}	1.8×10^{-9}	1.5×10^{-9}	5.1×10^{-9}	1.8×10^{-10}	1.9×10^{-9}	1.1×10^{-8}

Table 6. Dose at 5-cm Depth

Source	Incident Energy (MeV)	Dose (rads per nucleon/cm^2)						
		Protons at					Heavy Particles	Total
		0-1 MeV	1-5 MeV	5-10 MeV	10-50 MeV	> 50 MeV		
Normally incident protons	400	3.5×10^{-10}	1.1×10^{-9}	9.0×10^{-10}	3.3×10^{-9}	4.9×10^{-8}	1.3×10^{-9}	5.6×10^{-8}
	300	3.6×10^{-10}	1.1×10^{-9}	9.8×10^{-10}	3.7×10^{-9}	5.6×10^{-8}	1.5×10^{-9}	6.4×10^{-8}
	200	3.9×10^{-10}	1.3×10^{-9}	1.0×10^{-9}	4.2×10^{-9}	7.8×10^{-8}	1.3×10^{-9}	8.6×10^{-8}
	100	5.0×10^{-10}	1.7×10^{-9}	1.4×10^{-9}	6.8×10^{-9}	1.7×10^{-7}	1.1×10^{-9}	1.8×10^{-7}
	60	-	-	-	-	-	-	-
Normally incident neutrons	400	2.9×10^{-10}	9.0×10^{-10}	7.0×10^{-10}	2.3×10^{-9}	3.2×10^{-9}	1.6×10^{-9}	9.0×10^{-9}
	300	3.2×10^{-10}	9.5×10^{-10}	8.0×10^{-10}	2.9×10^{-9}	3.3×10^{-9}	1.5×10^{-9}	9.8×10^{-9}
	200	3.2×10^{-10}	1.0×10^{-9}	8.0×10^{-10}	2.9×10^{-9}	3.3×10^{-9}	1.5×10^{-9}	9.8×10^{-9}
	100	4.0×10^{-10}	1.2×10^{-9}	9.6×10^{-10}	4.0×10^{-9}	1.8×10^{-9}	1.6×10^{-9}	1.0×10^{-8}
	60	4.5×10^{-10}	1.4×10^{-9}	1.2×10^{-9}	4.2×10^{-9}	1.8×10^{-10}	1.2×10^{-9}	8.6×10^{-9}
Isotropically incident protons	400	6.5×10^{-10}	2.2×10^{-9}	2.0×10^{-9}	9.5×10^{-9}	1.0×10^{-7}	2.3×10^{-9}	1.2×10^{-7}
	300	7.0×10^{-10}	2.3×10^{-9}	2.1×10^{-9}	1.0×10^{-8}	1.1×10^{-7}	2.0×10^{-9}	1.3×10^{-7}
	200	8.5×10^{-10}	2.8×10^{-9}	4.0×10^{-9}	1.6×10^{-8}	1.3×10^{-7}	1.8×10^{-9}	1.6×10^{-7}
	100	3.0×10^{-9}	1.2×10^{-8}	1.4×10^{-8}	1.4×10^{-7}	1.4×10^{-8}	2.5×10^{-10}	1.8×10^{-7}
	60	-	-	-	-	-	-	-
Isotropically incident neutrons	400	7.0×10^{-10}	2.2×10^{-9}	1.8×10^{-9}	7.0×10^{-9}	1.2×10^{-8}	3.0×10^{-9}	2.7×10^{-8}
	300	7.0×10^{-10}	2.3×10^{-9}	1.9×10^{-9}	7.5×10^{-9}	1.1×10^{-8}	2.8×10^{-9}	2.6×10^{-8}
	200	7.2×10^{-10}	2.3×10^{-9}	1.8×10^{-9}	7.0×10^{-9}	8.3×10^{-9}	2.7×10^{-9}	2.3×10^{-8}
	100	7.0×10^{-10}	2.3×10^{-9}	1.8×10^{-9}	7.2×10^{-9}	3.2×10^{-9}	2.4×10^{-9}	1.8×10^{-8}
	60	7.3×10^{-10}	2.3×10^{-9}	2.0×10^{-9}	6.8×10^{-9}	2.6×10^{-10}	2.3×10^{-9}	1.4×10^{-8}

Table 7. Surface Dose

Source	Incident Energy (MeV)	Dose (rads per nucleon/cm²)						
		Protons at					Heavy Particles	Total
		0-1 MeV	1-5 MeV	5-10 MeV	10-50 MeV	> 50 MeV		
Normally incident protons	400	1.6×10^{-10}	5.0×10^{-10}	3.6×10^{-10}	1.5×10^{-9}	4.9×10^{-8}	1.1×10^{-9}	5.3×10^{-8}
	300	2.9×10^{-10}	8.8×10^{-10}	7.6×10^{-10}	1.6×10^{-9}	5.6×10^{-8}	1.5×10^{-9}	6.1×10^{-8}
	200	2.7×10^{-10}	6.5×10^{-10}	5.0×10^{-10}	1.7×10^{-9}	7.5×10^{-8}	1.3×10^{-9}	7.9×10^{-8}
	100	3.2×10^{-10}	1.0×10^{-9}	7.8×10^{-10}	1.1×10^{-9}	1.2×10^{-7}	1.1×10^{-9}	1.2×10^{-7}
	60	3.0×10^{-10}	9.0×10^{-10}	5.5×10^{-10}	2.0×10^{-8}	1.7×10^{-7}	2.2×10^{-10}	1.7×10^{-7}
Normally incident neutrons	400	2.2×10^{-10}	7.4×10^{-10}	5.0×10^{-10}	1.3×10^{-9}	6.0×10^{-10}	1.5×10^{-9}	4.9×10^{-9}
	300	1.7×10^{-10}	5.5×10^{-10}	4.0×10^{-10}	1.1×10^{-9}	3.0×10^{-10}	3.0×10^{-9}	3.8×10^{-9}
	200	2.2×10^{-10}	6.5×10^{-10}	4.2×10^{-10}	1.0×10^{-9}	2.0×10^{-10}	1.1×10^{-9}	3.6×10^{-9}
	100	2.8×10^{-10}	7.5×10^{-10}	5.0×10^{-10}	8.0×10^{-10}	3.0×10^{-10}	1.3×10^{-9}	3.9×10^{-9}
	60	2.6×10^{-10}	8.0×10^{-10}	6.0×10^{-10}	2.0×10^{-9}	1.2×10^{-10}	1.0×10^{-9}	4.8×10^{-9}
Isotropically incident protons	400	5.5×10^{-10}	1.6×10^{-9}	1.4×10^{-9}	6.0×10^{-9}	1.1×10^{-7}	2.3×10^{-9}	1.2×10^{-7}
	300	4.5×10^{-10}	1.4×10^{-9}	1.2×10^{-9}	4.2×10^{-9}	1.2×10^{-7}	2.0×10^{-9}	1.3×10^{-7}
	200	5.4×10^{-10}	1.8×10^{-9}	2.0×10^{-9}	5.4×10^{-9}	1.5×10^{-7}	2.1×10^{-9}	1.6×10^{-7}
	100	7.0×10^{-10}	2.0×10^{-9}	2.0×10^{-9}	1.0×10^{-8}	2.3×10^{-7}	1.8×10^{-9}	2.5×10^{-7}
	60	2.0×10^{-9}	7.0×10^{-9}	9.0×10^{-9}	1.8×10^{-7}	1.7×10^{-7}	7.0×10^{-10}	3.7×10^{-7}
Isotropically incident neutrons	400	6.2×10^{-10}	1.8×10^{-9}	1.5×10^{-9}	5.4×10^{-9}	7.0×10^{-9}	3.0×10^{-9}	1.9×10^{-8}
	300	5.0×10^{-10}	1.6×10^{-9}	1.2×10^{-9}	3.8×10^{-9}	4.0×10^{-9}	2.5×10^{-9}	1.4×10^{-8}
	200	5.2×10^{-10}	1.7×10^{-9}	1.1×10^{-9}	4.0×10^{-9}	3.0×10^{-9}	2.7×10^{-9}	1.3×10^{-8}
	100	5.6×10^{-10}	1.5×10^{-9}	1.1×10^{-9}	3.5×10^{-9}	1.5×10^{-9}	2.4×10^{-9}	1.0×10^{-8}
	60	7.6×10^{-10}	2.3×10^{-9}	2.0×10^{-9}	6.4×10^{-9}	3.0×10^{-10}	2.2×10^{-9}	1.4×10^{-8}

Table 8. Maximum Dose

Source	Incident Energy (MeV)	Dose (rads per nucleon/cm²)					Heavy Particles	Total
		Protons at						
		0-1 MeV	1-5 MeV	5-10 MeV	10-50 MeV	> 50 MeV		
Normally incident protons	400	4.7×10^{-10}	1.5×10^{-9}	1.3×10^{-9}	6.6×10^{-9}	5.2×10^{-8}	1.7×10^{-9}	6.4×10^{-8}
	300	4.5×10^{-10}	1.5×10^{-9}	1.3×10^{-9}	6.6×10^{-9}	6.6×10^{-8}	1.5×10^{-9}	7.7×10^{-8}
	200	1.2×10^{-8}	4.7×10^{-8}	5.9×10^{-8}	2.6×10^{-7}	-	-	3.8×10^{-7}
	100	1.5×10^{-8}	5.9×10^{-8}	7.3×10^{-8}	3.3×10^{-7}	-	-	4.8×10^{-7}
	60	1.6×10^{-8}	6.3×10^{-8}	7.8×10^{-8}	3.5×10^{-7}	0	0	5.1×10^{-7}
Normally incident neutrons	400	4.0×10^{-10}	1.3×10^{-9}	1.1×10^{-9}	4.8×10^{-9}	1.0×10^{-8}	2.0×10^{-9}	1.9×10^{-8}
	300	4.0×10^{-10}	1.3×10^{-9}	1.1×10^{-9}	4.8×10^{-9}	8.6×10^{-9}	1.9×10^{-9}	1.8×10^{-8}
	200	4.0×10^{-10}	1.3×10^{-9}	1.1×10^{-9}	5.0×10^{-9}	6.0×10^{-9}	1.8×10^{-9}	1.6×10^{-8}
	100	4.5×10^{-10}	1.3×10^{-9}	1.1×10^{-9}	4.5×10^{-9}	2.0×10^{-9}	1.8×10^{-9}	1.1×10^{-8}
	60	4.5×10^{-10}	1.4×10^{-9}	1.2×10^{-9}	4.2×10^{-9}	1.8×10^{-10}	1.2×10^{-9}	8.6×10^{-9}
Isotropically incident protons	400	6.5×10^{-10}	2.2×10^{-9}	2.0×10^{-9}	9.5×10^{-9}	1.0×10^{-7}	2.3×10^{-9}	1.2×10^{-7}
	300	7.0×10^{-10}	2.3×10^{-9}	2.1×10^{-9}	1.0×10^{-8}	1.1×10^{-7}	2.0×10^{-9}	1.3×10^{-7}
	200	8.5×10^{-10}	2.8×10^{-9}	4.0×10^{-9}	1.6×10^{-8}	1.3×10^{-7}	1.8×10^{-9}	1.6×10^{-7}
	100	2.1×10^{-9}	8.0×10^{-9}	1.0×10^{-8}	9.5×10^{-8}	1.4×10^{-7}	1.1×10^{-9}	2.6×10^{-7}
	60	2.0×10^{-9}	7.0×10^{-9}	9.0×10^{-9}	1.8×10^{-7}	1.7×10^{-7}	7.0×10^{-10}	3.7×10^{-7}
Isotropically incident neutrons	400	7.5×10^{-10}	2.3×10^{-9}	2.0×10^{-9}	8.5×10^{-9}	1.7×10^{-8}	3.0×10^{-9}	3.4×10^{-8}
	300	7.2×10^{-10}	2.2×10^{-9}	1.9×10^{-9}	8.0×10^{-9}	1.3×10^{-8}	2.7×10^{-9}	2.9×10^{-8}
	200	7.2×10^{-10}	2.3×10^{-9}	1.9×10^{-9}	8.5×10^{-9}	1.0×10^{-8}	2.6×10^{-9}	2.6×10^{-8}
	100	7.5×10^{-10}	2.3×10^{-9}	1.9×10^{-9}	7.8×10^{-9}	3.2×10^{-9}	2.4×10^{-9}	1.8×10^{-8}
	60	7.6×10^{-10}	2.3×10^{-9}	2.0×10^{-9}	6.4×10^{-9}	3.0×10^{-10}	2.2×10^{-9}	1.9×10^{-8}

properly by the computer. For this reason the maximum dose data (which is an average over the last centimeter of path in the case of protons) presented in Table 8 for normally incident, 60-, 100-, and 200-MeV protons were calculated by hand from detailed data not ordinarily part of the output.

As a test of the applicability of the current-to-dose conversion factors, Irving et al.[20] computed the dose in tissue behind various shields. Monoenergetic protons were incident isotropically on the shield, and the dose in the tissue was calculated both directly by using Monte Carlo methods and by means of the above factors. It was found that in general the doses resulting from applying the factors did indeed bracket those directly calculated.

V. CONCLUSIONS

Assuming Shalnov's neutron experiments to be correct, the comparisons indicate that our calculations of the dose in tissue due to neutrons below 400 MeV are good to within a factor of 2, at worst. They may well be better than this since the differences between the experimental arrangement and the calculational model, along with some experimental unknowns, could account for the discrepancies.

Neutrons can only deposit energy indirectly by means of the secondary charged particles produced. Thus a comparison with a neutron dose experiment is a test of the integral effects of the calculated secondary production. The calculated secondary production due to neutrons and protons is roughly the same. Therefore, the calculated proton doses should be uncertain to 50% at most because the secondaries contribute no more than half the total proton dose and there is little uncertainty in the energy deposited by the

primary proton beam through ionization. More experimental information is clearly needed to check the calculations further.

The calculations show that, for the energy range considered, neutron and proton fluxes up to four times higher than those estimated by Neary and Mulvey[1] may be tolerated without exceeding 0.3 rem/40 hr.

Calculated doses due to 10-MeV neutrons agree with previous calculations[13] when the same assumptions are made. The inclusion of the anisotropy of neutron elastic scattering from the tissue nuclei, however, was found to reduce the heavy recoil dose by a factor of about 2 and so should be included in the calculations.

The most striking feature of this calculation is the significant contribution that the heavy-particle recoils make to the rem dose for the case of incident neutrons or protons. In the case of incident protons the contribution is in general of the order of 10 to 20%, but for incident neutrons it constitutes the greatest fraction of the total contribution. Unfortunately, the rad dose from the heavy particles was converted to rem dose using a QF from the high-LET and most suspicious portion of the QF vs LET curve shown in Fig. 3. This points up the necessity of establishing the QF factors with some degree of accuracy for high-LET values if any reasonable degree of accuracy is to be obtained in the current-to-rem dose conversion factors.

As a consequence of the significant contribution of the heavy particles and secondary protons to the rem dose, it is not reasonable to expect that the rem dose at any depth from incident protons can be calculated very accurately unless the secondary radiation created in the body is taken into consideration. For the case of incident neutrons this is obviously true because only through secondary radiations is it possible for neutrons to deposit energy.

REFERENCES

1. G. J. Neary and J. Mulvey, _Maximum Permissible Fluxes of High Energy Neutrons and Protons in the Range 40 to 1000 MeV_, Medical Research Council of Radiological Research Unit, A.E.R.E. Harwell (unpublished).

2. J. E. Turner _et al._, _Health Phys._ 10, 783 (1964).

3. H. J. Shaefer, U. S. Naval School of Aviation Medicine, Pensacola, private communication.

4. M. I. Shalnov, _Soviet J. At. Energy_ 5,735 (1958).

5. See the Appendix, p. 56.

6. W. E. Kinney, R. R. Coveyou, and C. D. Zerby, p. 608 in _Proceedings of the Symposium on the Protection Against Radiation Hazards in Space, Gatlinburg, Tennessee, November 5-7, 1962_, TID-7652, Book 2; W. E. Kinney, _The Nucleon Transport Code, NTC_, Oak Ridge National Laboratory Report ORNL-3610 (August 1964).

7. H. Bethe and J. Ashkin, _Experimental Nuclear Physics_, Part II (E. Segrè, ed.), Wiley, New York, 1953.

8. H. W. Bertini, _Phys. Rev._ 131, 1801 (1963).

9. L. Dresner, _EVAP - A Fortran Program for Calculating the Evaporation of Various Particles from Excited Compound Nuclei_, Oak Ridge National Laboratory Report ORNL CF-61-12-30.

10. I. Dostrovsky, Z. Fraenkel, and G. Friedlander, _Phys. Rev._ 116, 683 (1959); I. Dostrovsky, Z. Fraenkel, and L. Winsberg, _Phys. Rev._ 118, 781 (1960); and I. Dostrovsky, Z. Fraenkel, and P. Robinowitz, _Phys. Rev._ 118, 791 (1960).

11. R. R. Coveyou, J. G. Sullivan, and H. P. Carter, p. 267 in _Codes for Reactor Computations_, International Atomic Energy Agency, Vienna, 1961; R. R. Coveyou _et al._, _O5R: A General Purpose Monte Carlo Neutron Transport Code_, Oak Ridge National Laboratory Report ORNL-3622 (1965).

12. M. D. Goldberg, V. M. May, and J. R. Stehn, _Angular Distributions in Neutron Induced Reactions_, Vol. 1, Brookhaven National Laboratory Report BNL-400 (October 1962).

13. W. Snyder and J. Neufeld, _Brit. J. Radiol._ 28, 342 (1955).

14. "Recommendations of the International Commission on Radiological Protection and of the International Commission on Radiological Units," _Natl. Bur. Std. (U.S.) Handbook_ 47, 16 (1950).

References (Contd.)

15. "Permissible Dose from External Sources of Ionizing Radiation," Natl. Bur. Std. (U.S.) Handbook, Vol. 59 (1954).

16. "Report of the RBE Committee to the International Commissions on Radiological Protection and on Radiological Units and Measurements," Health Phys. 9, 357 (1963).

17. P. R. Serber, Phys. Rev. 72, 1008 (1947).

18. V. P. Dzhelepov et al., Izv. Akad. Nauk SSSR Ser. Fiz. 19, 573 (1955).

19. "Protection Against Neutron Radiation up to 30 Million Electron Volts," Natl. Bur. Std. (U.S.) Handbook Vol. 63 (1957).

20. D. C. Irving, R. G. Alsmiller, Jr., W. E. Kinney, and H. S. Moran, "The Secondary-Particle Contribution to the Dose from Monoenergetic Proton Beams and the Validity of Flux-to-Dose Conversion Factors," to be published in Proceedings of the Second Symposium on Protection Against Radiation Hazards in Space, Gatlinburg, Tennessee, October 12-14, 1964.

APPENDIX.   RAD DOSE AS A FUNCTION OF DEPTH IN TISSUE

The energy deposition data presented in the text are for the average whole-body dose, the doses on the surface and at a 5-cm depth, and the maximum dose. Since complete information about the energy deposition as a function of depth in tissue may be of value in some instances, the detailed data are included in this appendix. These data were generated for the 30-cm-thick model of the body and the monoenergetic broad-beam source described in the text. All the data for source energies up to 400 MeV are presented for both isotropically and normally incident nucleons.

The energy deposition data are divided into contributions from primary protons, secondary protons, and heavy nuclei. The proton doses are further subdivided into contributions due to protons in the energy ranges 0-1, 1-5, 5-10, 10-50, and > 50 MeV so that arbitrary QF's can be used in arriving at a rem dose. The units used for reporting the energy deposition is the rad (1 rad = 100 ergs/g).

The estimates of dose were obtained by averaging the energy deposition over 1-cm subslabs. The estimates were subject to the statistical fluctuations inherent in Monte Carlo calculations, as may be seen in **Figs. 9** through 12 of the text. The curves were obtained simply by fitting a curve through the Monte Carlo data by eye. Total and partial doses were fitted separately so that the total curves may not in all cases be exactly equal to the sum of the partial doses.

Figure Al gives the dose as a function of depth for 400-MeV protons normally incident in a broad beam. The dose due to the primary beam falls with increasing depth since the beam depletion through nuclear interactions
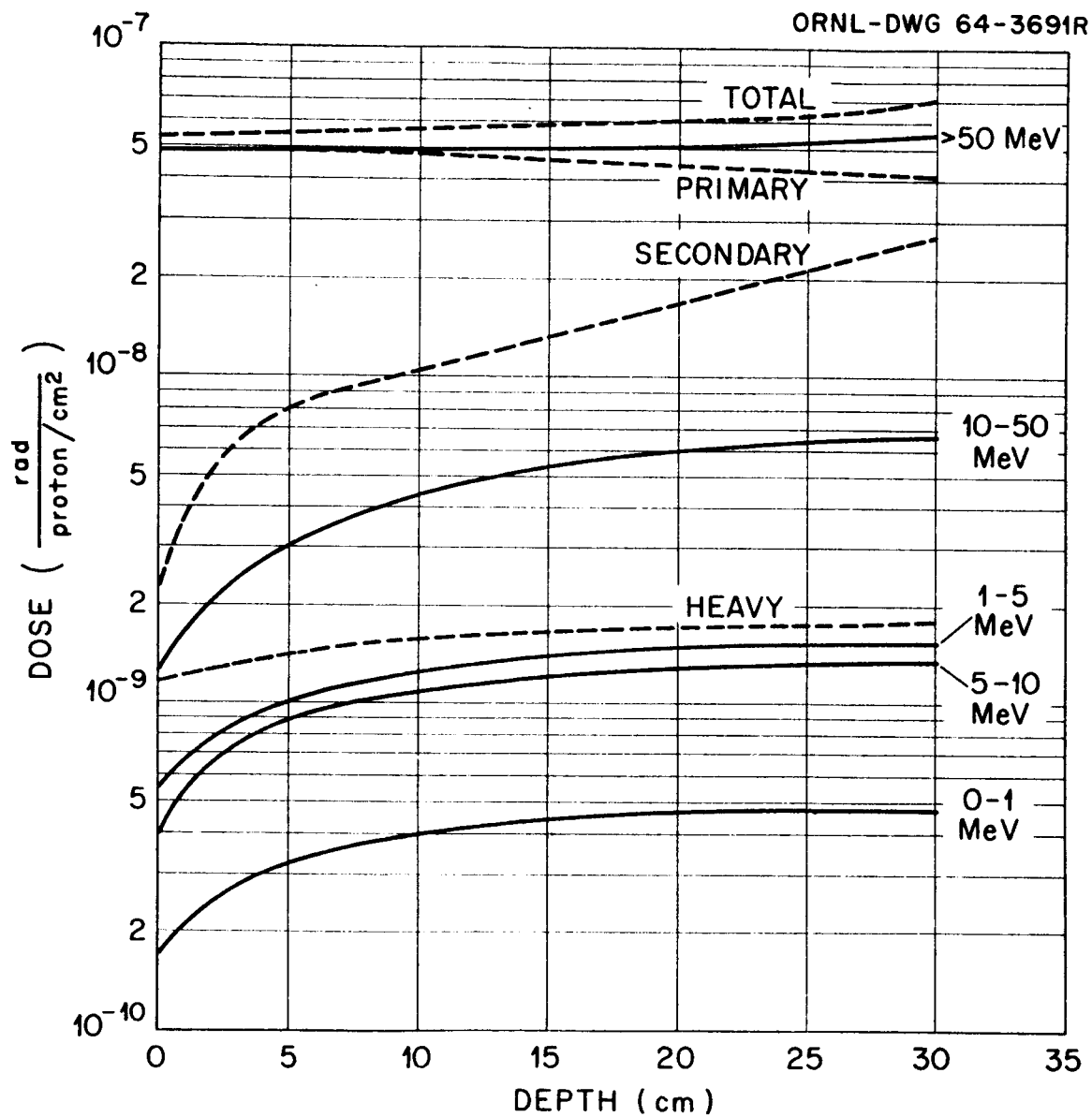
Fig. Al. Rad Dose vs Depth Due To 400-MeV Normally Incident Protons.

overrides the increasing stopping power as the primary energy decreases.
The secondary proton population builds up with increasing depth and this,
together with a larger stopping power associated with the lower energy
secondaries, causes the secondary proton dose to rise to within half the
primary dose at 30 cm. The partial secondary dose due to protons with
energies above 50 MeV reflects the secondary proton production and rises
with increasing depth. The other partial proton doses all rise rather
steeply, proceeding from the front surface to a depth of 10 cm as the
secondaries build up, slow down, and have interactions. The rise is more
gradual from 10 to 20 cm, and beyond 20 cm the dose tends to level off.
The heavy particle contribution is due to recoil nuclei and evaporated
particles with mass greater than 1 and, unlike protons which distribute
energy along their path, all are assumed to deposit their energy at their
site of birth. The heavy-particle dose, then, depends on both the colli-
sion density and the energy of collision and is rather flat, rising some-
what as the secondaries build up.

Although the heavy contribution to the rad dose is never larger than
5% of that of the primary beam, an assumed QF of 20 brings the heavy contri-
bution to the rem dose at 30 cm to a value about equal to that of the prim-
aries. The net effect of all the energy deposition processes is to produce
an increase in the rad dose from 5.3×10^{-8} at the surface to 7.0×10^{-8} at
30 cm.

Very much the same observations may be made concerning Fig. A2, which
gives the doses due to 300-MeV normally incident protons. The primary
beam depletion just balances the increase in stopping power as the prim-
aries lose energy in traversing the medium and produces a flat primary

ORNL-DWG 64-3692
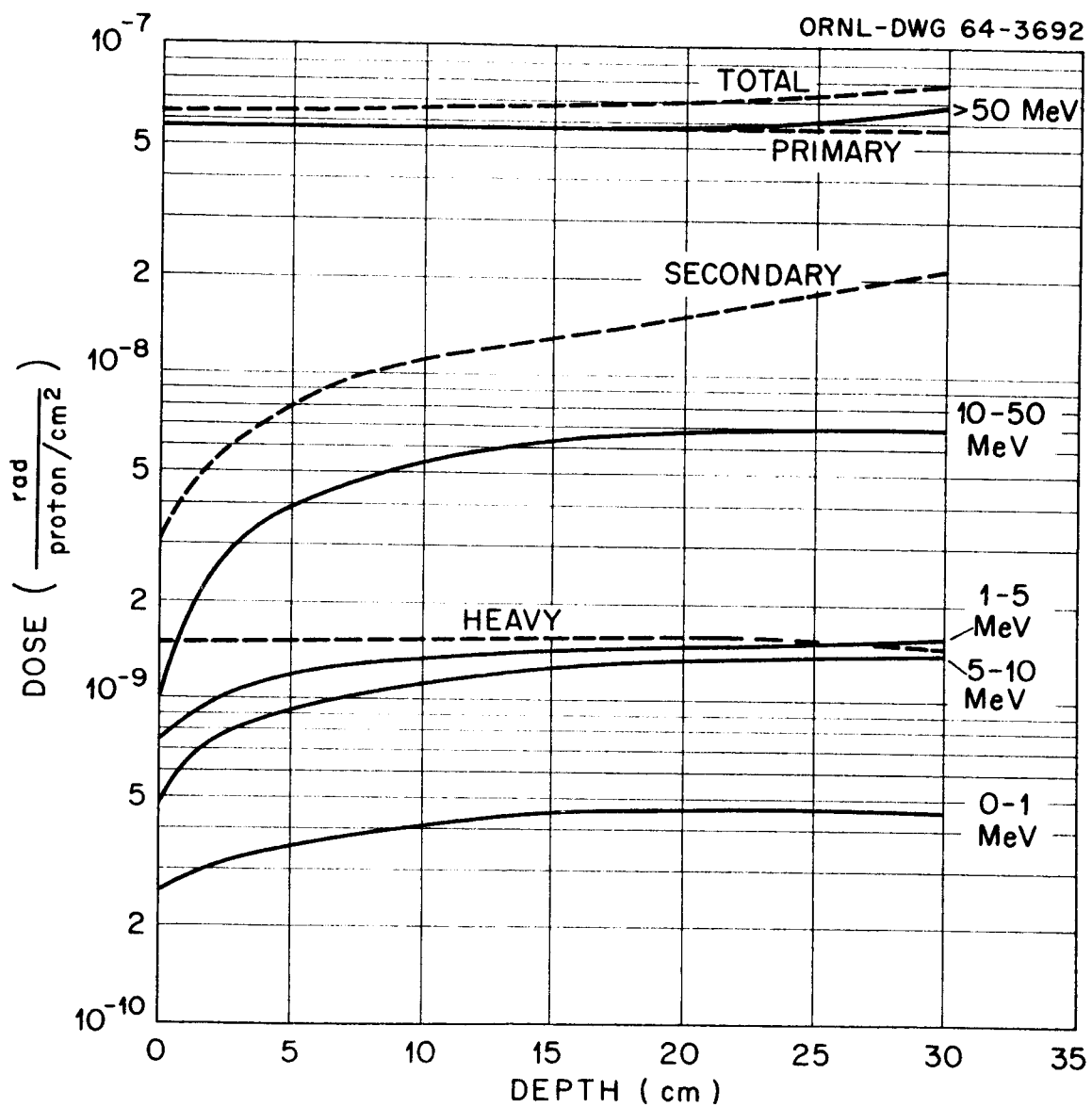
Fig. A2.   Rad Dose vs Depth Due To 300-MeV Normally Incident Protons.

contribution. The secondary contribution falls below that due to second-
aries for 400-MeV incident protons since nucleon multiplicities decrease
with decreasing energy.

Figure A3 shows the dose due to 200-MeV normally incident protons.
Protons of this energy have a range of about 25 cm in tissue of our
assumed composition, as may be seen from Fig. 1 of the text. The large
energy deposition at the end of the range represents an average over the
1-cm subslabs. No attempt was made to follow the energy deposition in any
finer detail.

Note that the assumption was made that protons below 50 MeV slow
down with no nuclear interactions. This accounts for the rapid fall
in secondary dose and in all but the 10- to 50-MeV partial proton doses
at about 22.5 cm. The partial proton doses rise to a large peak as the
primary beam passes through their respective energy intervals. Beyond
the range of the primary beam all the dose is due to interactions of
secondary neutrons born at smaller depths and is down by a factor of
roughly 80 below the dose at 15 cm.

The dose due to 100-MeV normally incident protons is given in Fig. A4.
The dose peaks occur here as at the 200-MeV incident energy only at a
depth of approximately 5 cm, the range to 50 MeV of 100-MeV protons in
tissue.

For simplicity, the doses due to 60-MeV normally incident protons
are given in tabular form in Table Al rather than as a plot. Nearly
all dose is due to ionization energy loss of the primary beam since it

ORNL-DWG 64-3693A
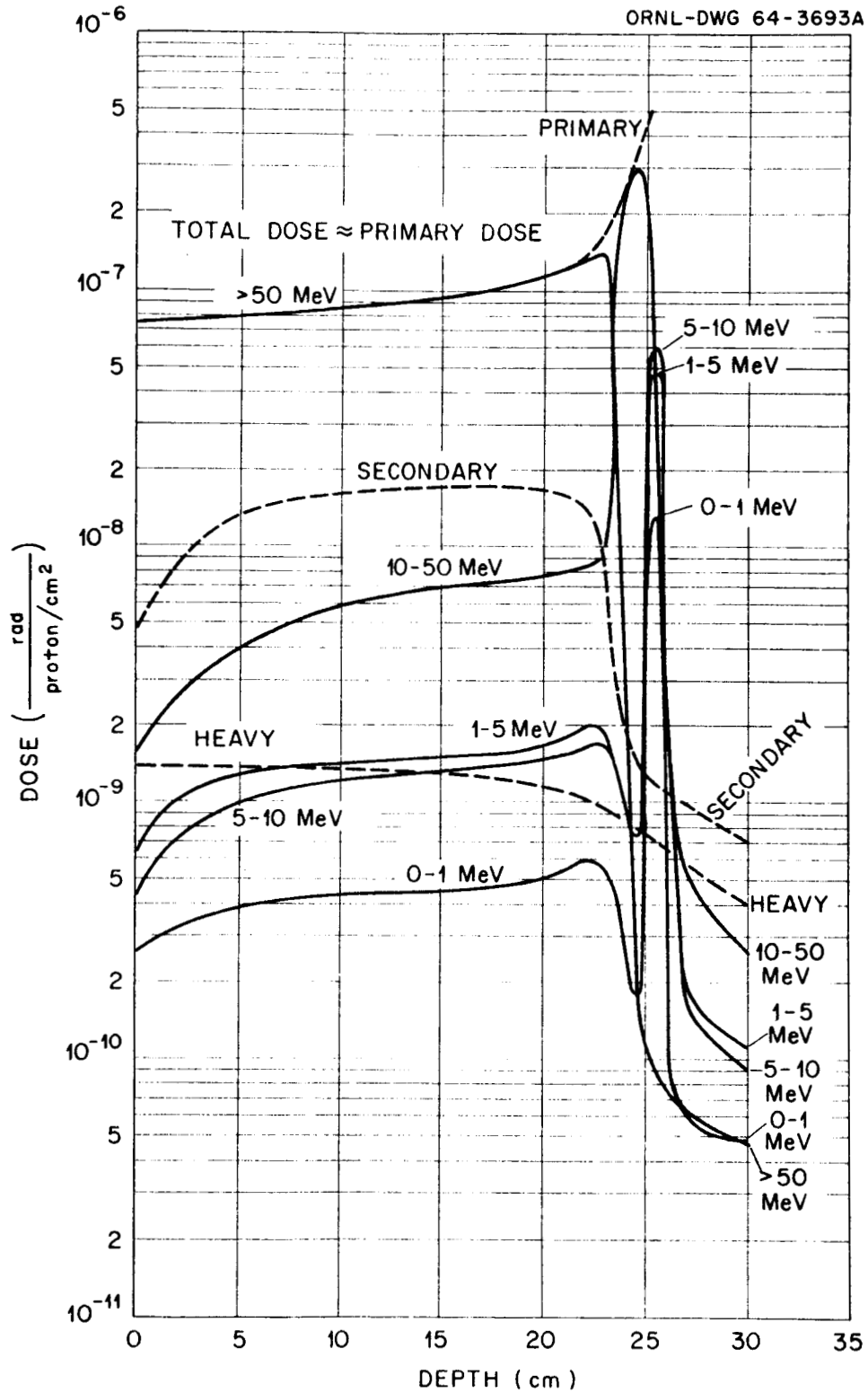
Fig. A3. Rad Dose vs Depth Due To 200-MeV Normally Incident Protons.
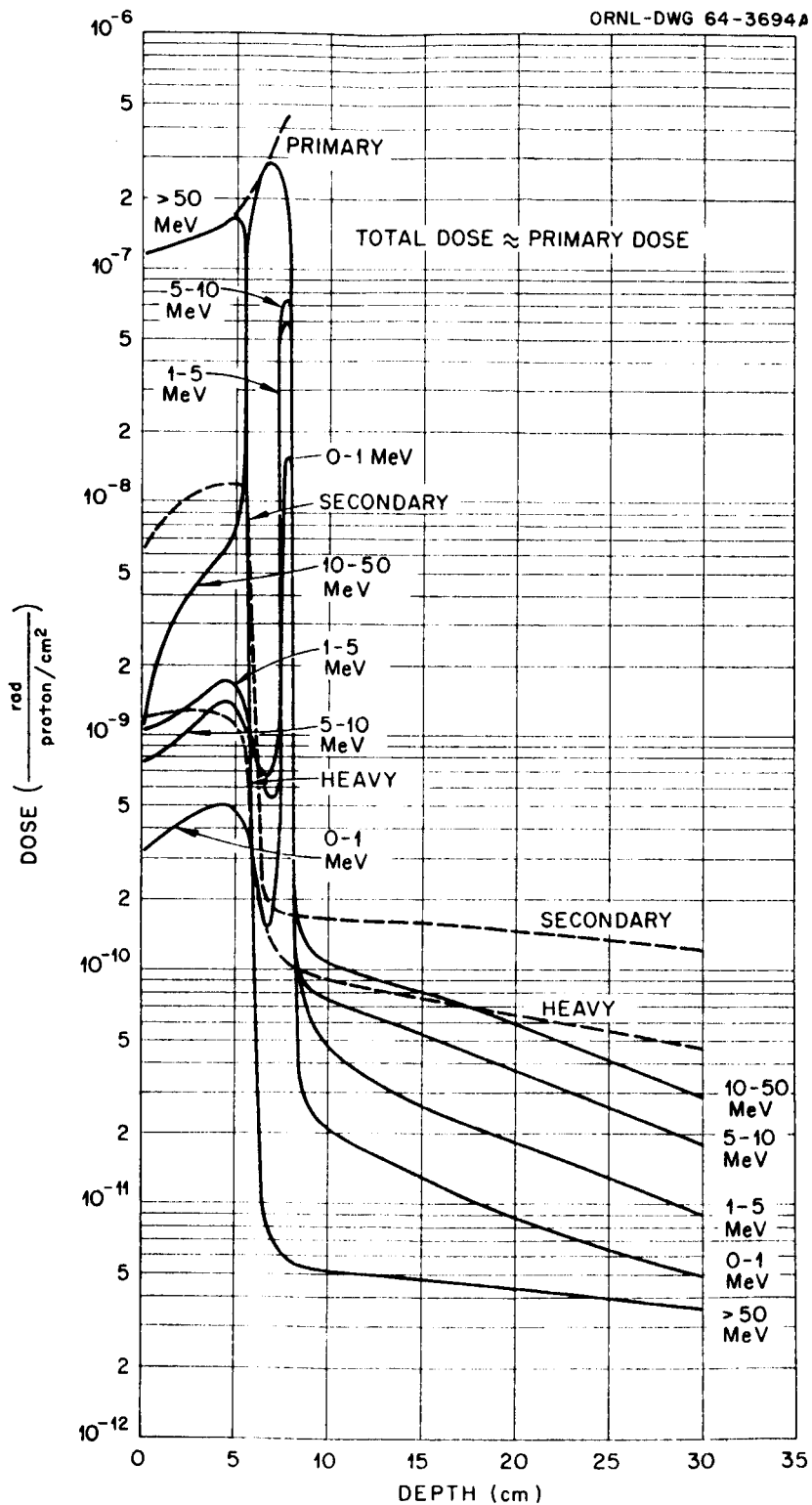
Fig. A4. Rad Dose vs Depth Due To 100-MeV Normally Incident Protons.

Table A1. Rad Dose as a Function of Depth in Tissue Due to 60-MeV Incident Protons

Depth (cm)	Primary Protons	Secondary Protons	Heavy Particles	Dose (in rads) Due to — Partial Protons of 0-1 MeV	1-5 MeV	5-10 MeV	>10 MeV
				Normally Incident Protons			
0-1	1.9×10^{-7}	5.1×10^{-9}	6.7×10^{-10}	2.5×10^{-10}	7.3×10^{-10}	5.1×10^{-10}	1.9×10^{-7}
1-2	2.5×10^{-7}	6.0×10^{-10}	8.6×10^{-13}	6.1×10^{-11}	2.4×10^{-10}	3.0×10^{-10}	2.5×10^{-7}
2-3	5.1×10^{-7}	-	-	1.6×10^{-8}	6.3×10^{-8}	7.9×10^{-8}	3.5×10^{-7}
				Isotropically Incident Protons			
0-1	3.8×10^{-7}	1.1×10^{-8}	7.0×10^{-10}	2.2×10^{-9}	8.6×10^{-9}	1.0×10^{-8}	3.7×10^{-7}
1-2	3.6×10^{-7}	9.9×10^{-9}	9.1×10^{-13}	5.9×10^{-9}	2.4×10^{-8}	3.0×10^{-8}	3.1×10^{-7}
2-3	2.1×10^{-7}	-	-	8.0×10^{-9}	3.2×10^{-8}	4.0×10^{-8}	1.3×10^{-7}

is assumed that protons below 50 MeV slow down with no nuclear interactions.

Doses due to normally incident neutrons of energy 400, 300, 200, 100, and 60 MeV are given in Figs. A5 through A9, respectively. The secondary production due to neutrons is roughly the same as that due to protons at 400 and 300 MeV, though the production due to the latter is somewhat higher since protons slow down and encounter higher cross sections as shown in Fig. 2 of the text. The neutron doses all display the same buildup at small depths due to secondary production. At lower incident energies, between 100 and 200 MeV, the dose goes through a maximum and falls, owing to primary depletion resulting from nuclear interactions and decreasing secondary production at lower energies. The magnitude of the dose falls slowly as the primary energy decreases since the smaller energy available for recoils and cascade particles is somewhat offset by the increasing cross sections.

Doses due to isotropically incident protons of energy 400, 300, 200, and 100 MeV are given in Figs. A10 through A13, respectively. In traversing a slab of given thickness, particles incident in a current distribution resulting from an isotropic flux on the average travel a distance equal to twice the thickness of the slab if there is no depletion. The isotropic doses are, then, nearly a factor of 2 higher at the surface than the doses resulting from normally incident protons, since the doses at the surface are almost entirely due to the primary proton ionization energy loss. This factor-of-2 relationship disappears within the slab because of the contribution from secondary production and the increasing stopping power with decreasing energy.
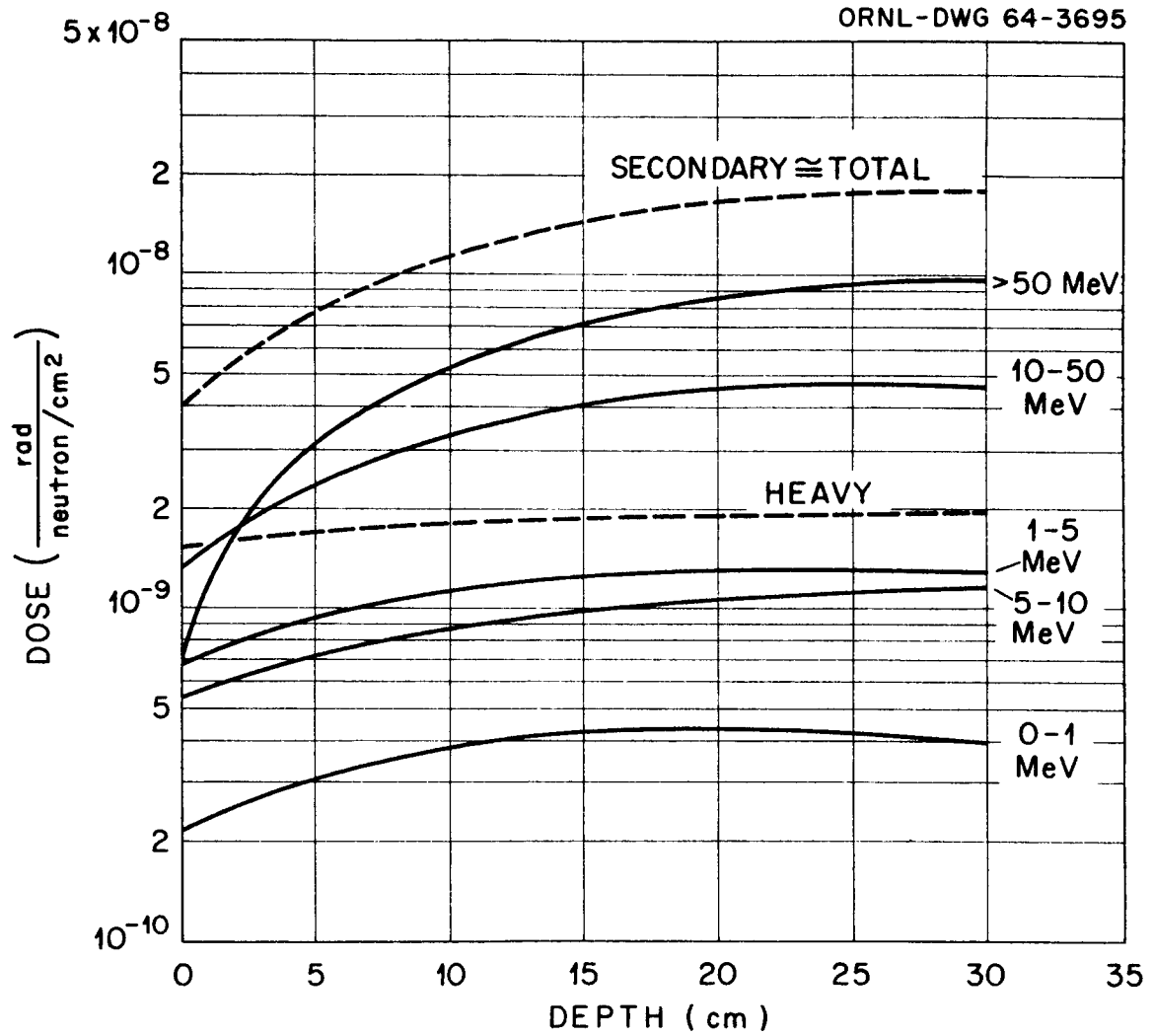
Fig. A5. Rad Dose vs Depth Due To 400-MeV Normally Incident Neutrons.
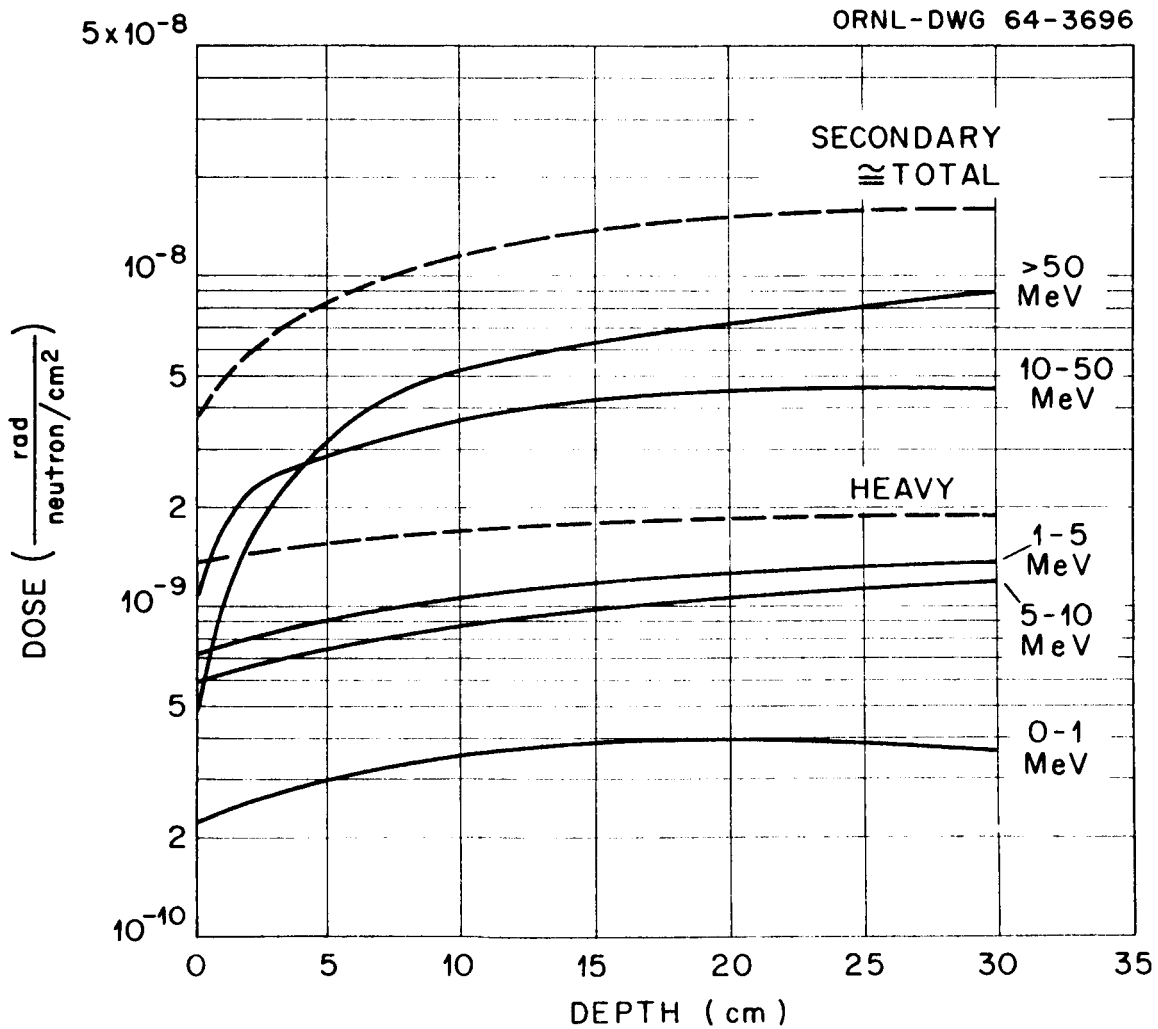
Fig. A6. Rad Dose vs Depth Due To 500-MeV Normally Incident Neutrons.
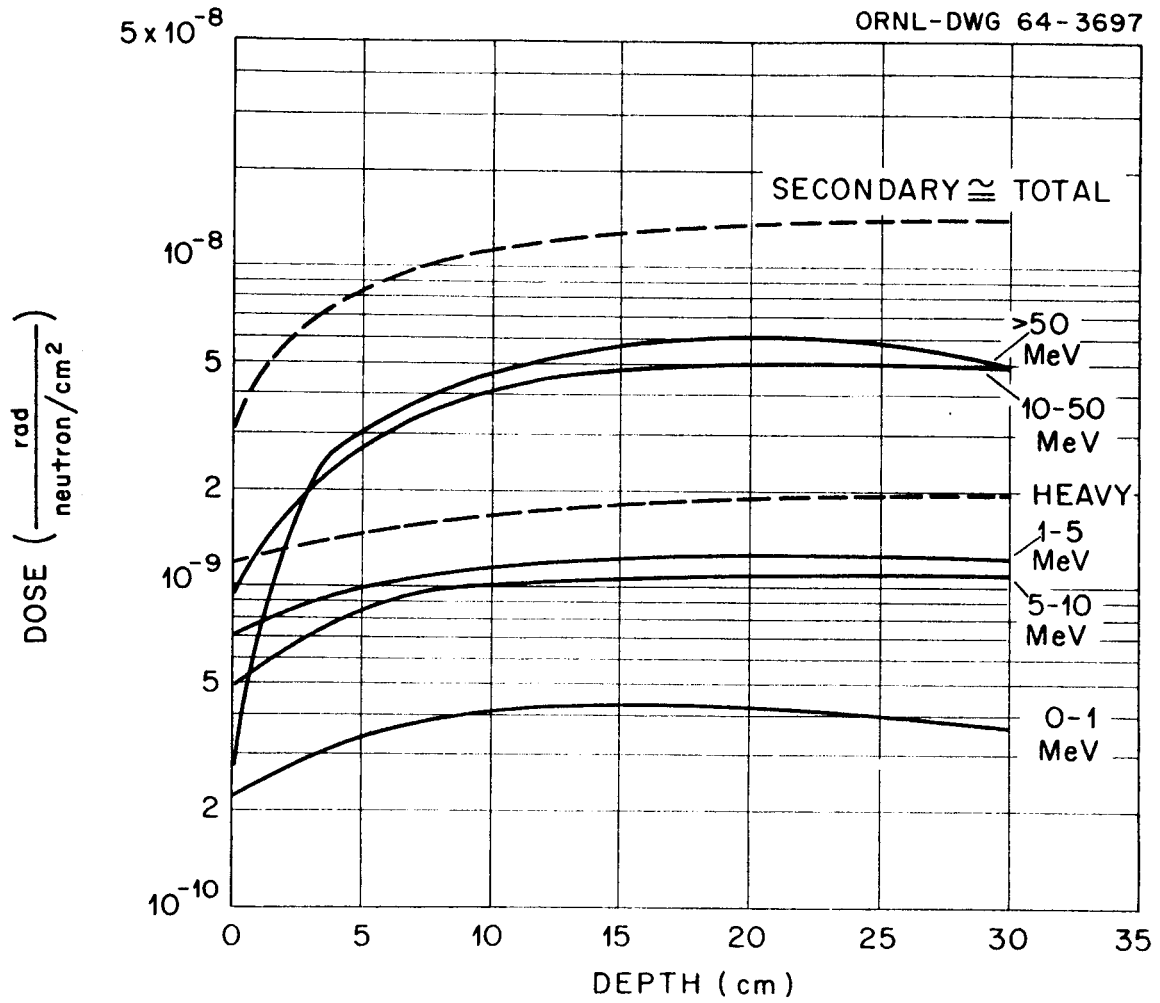
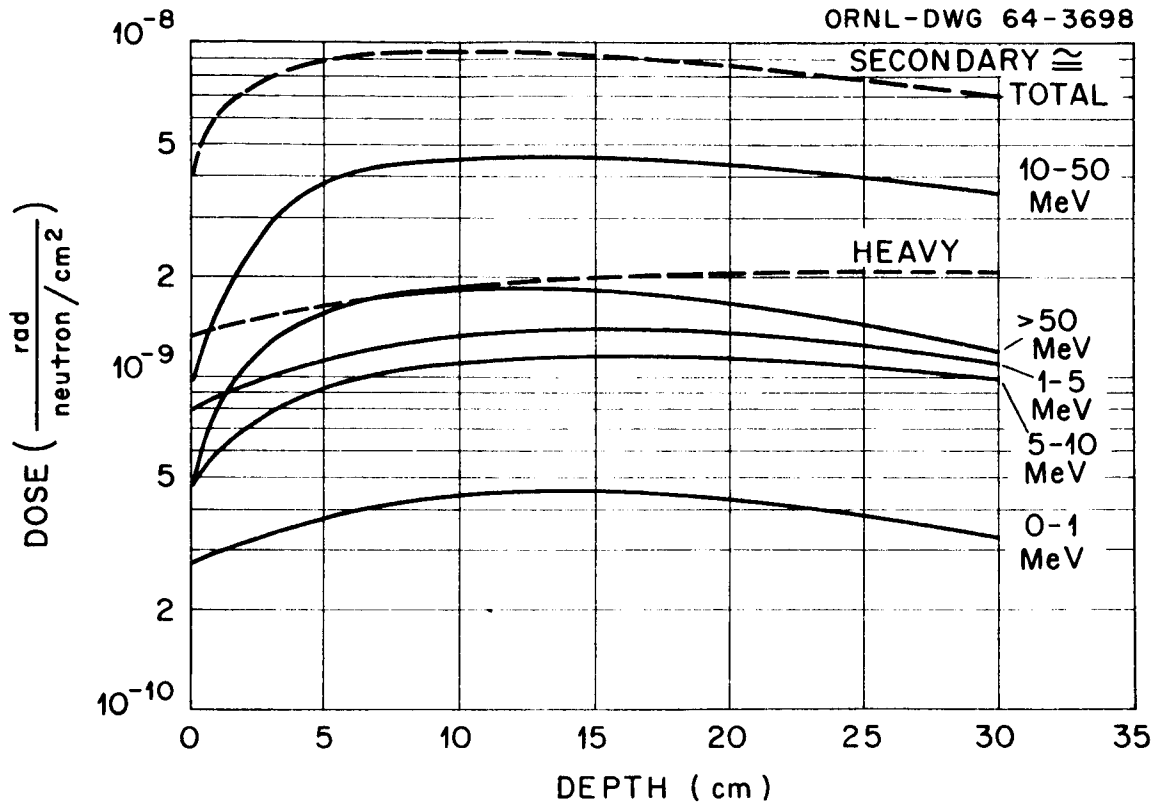Fig. A7. Rad Dose vs Depth Due To 200-MeV Normally Incident Neutrons.

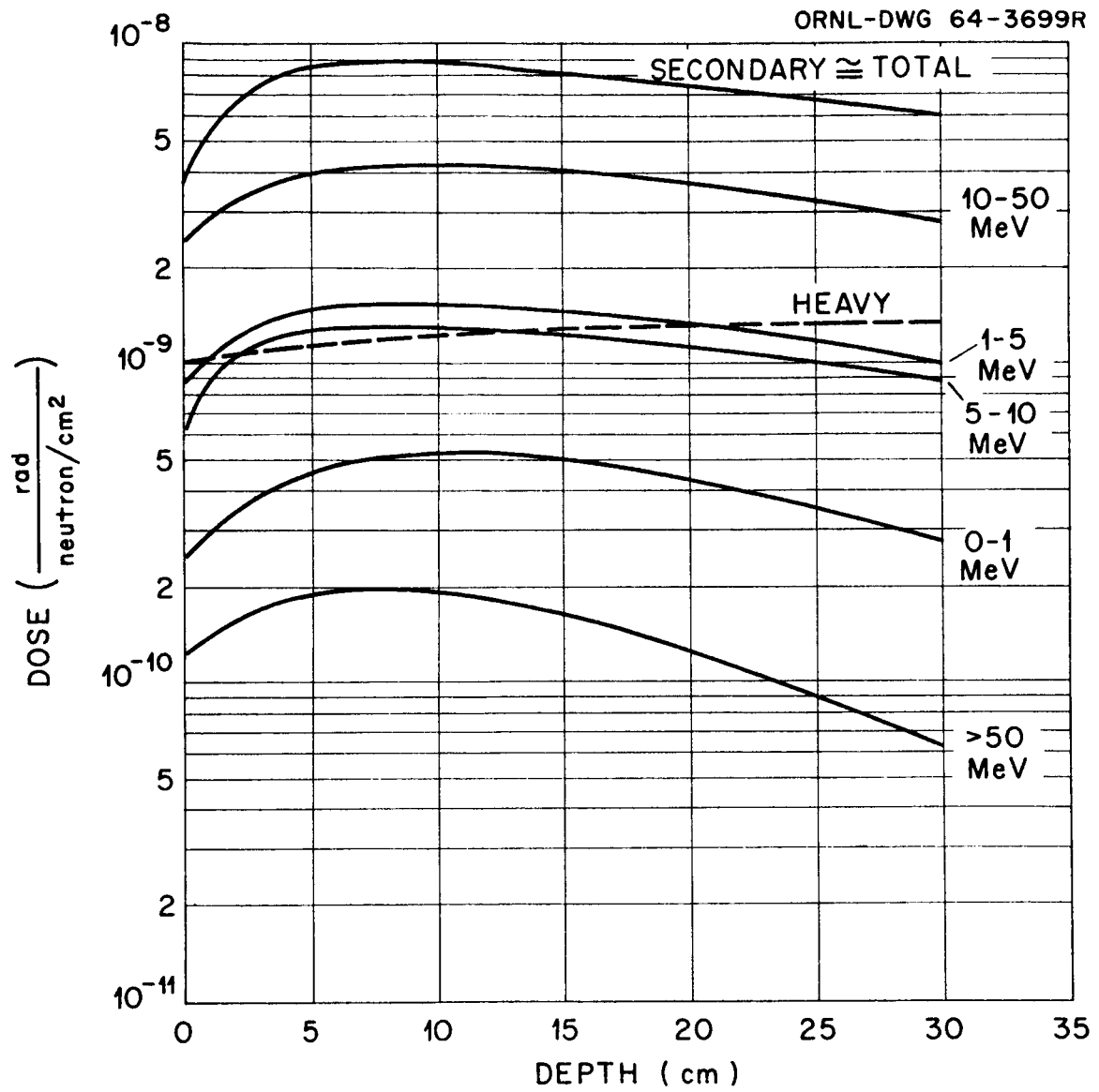Fig. A8. Rad Dose vs Depth Due To 100-MeV Normally Incident Neutrons.

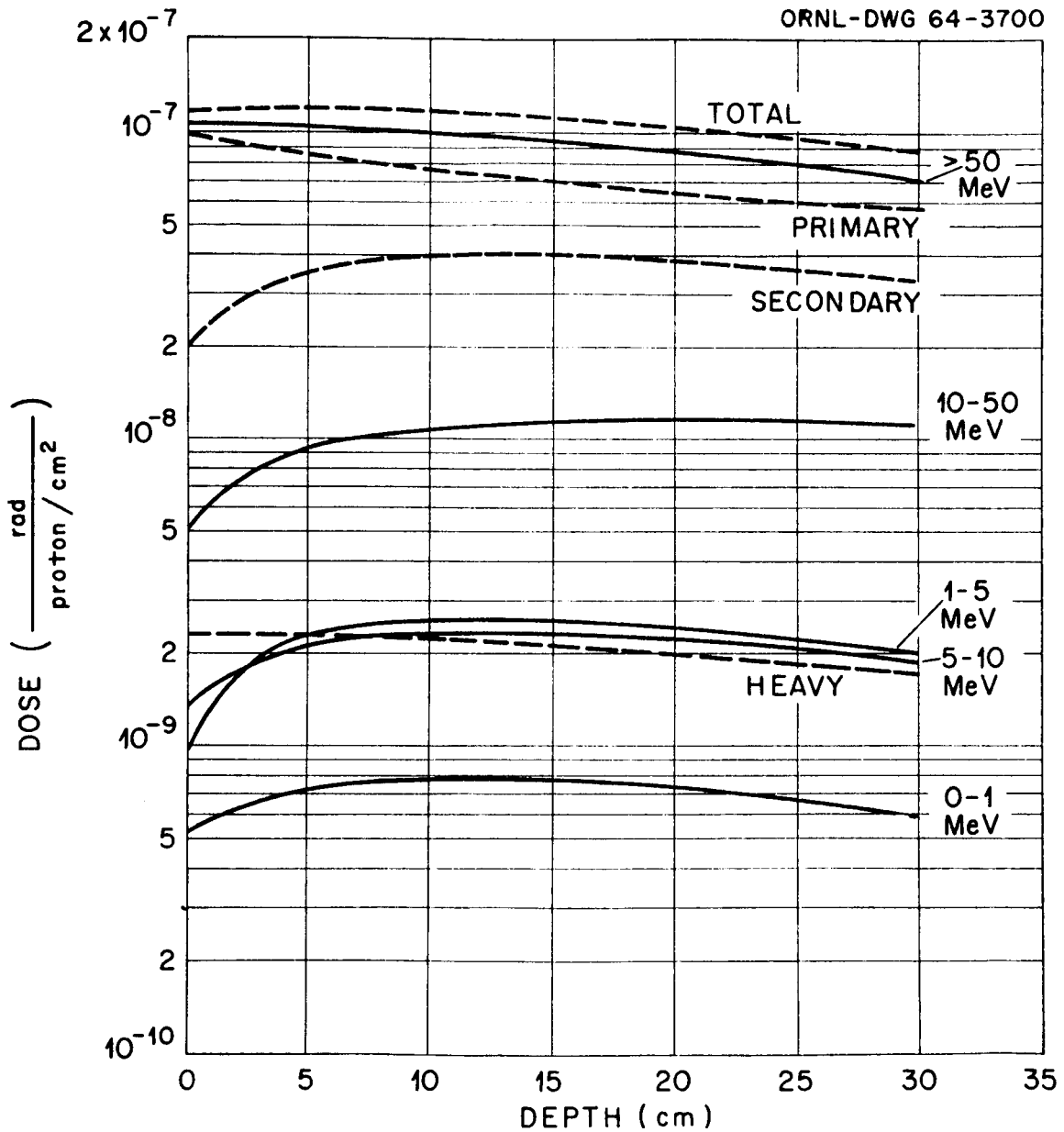Fig. A9. Rad Dose vs Depth Due To 60-MeV Normally Incident Neutrons.

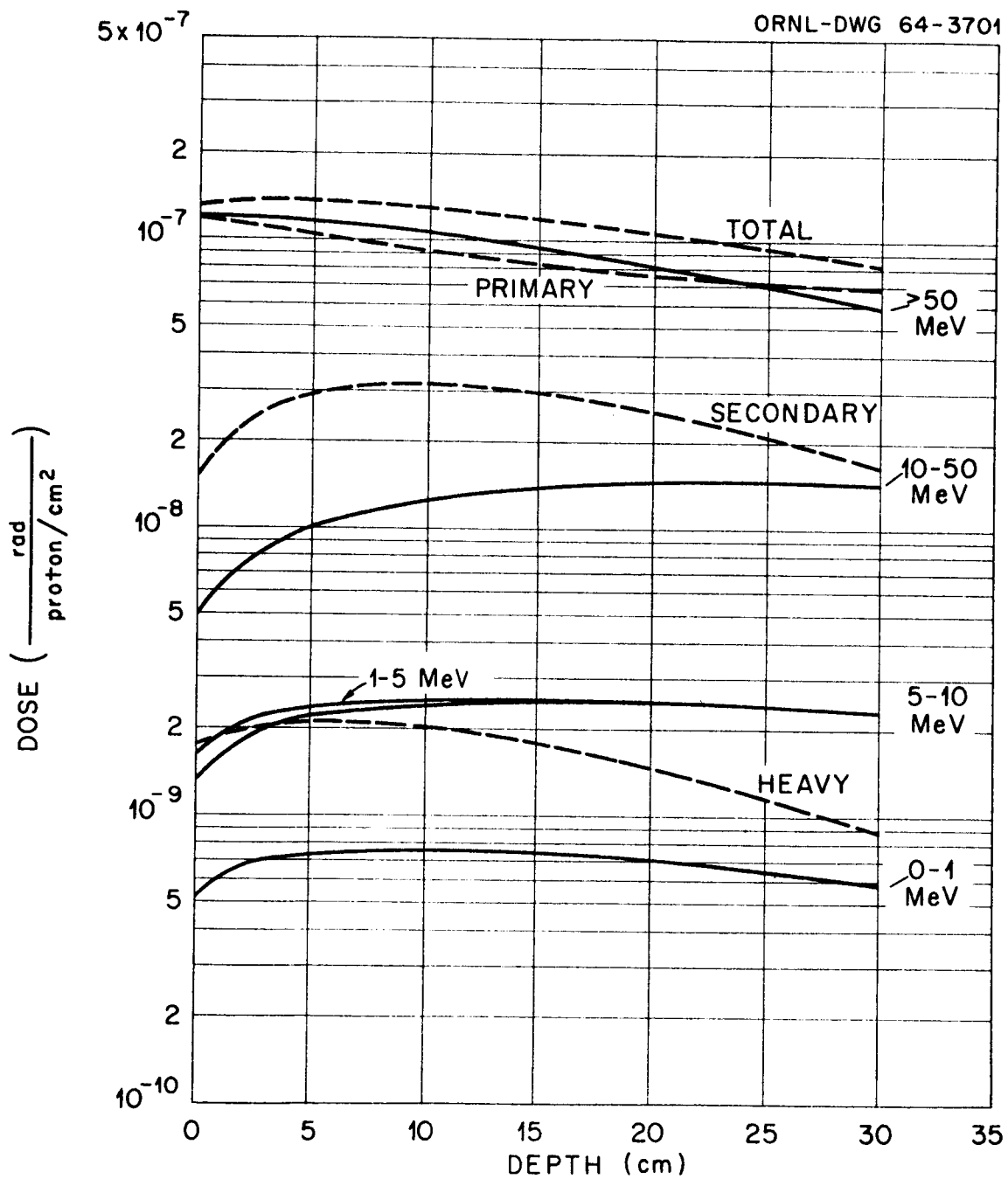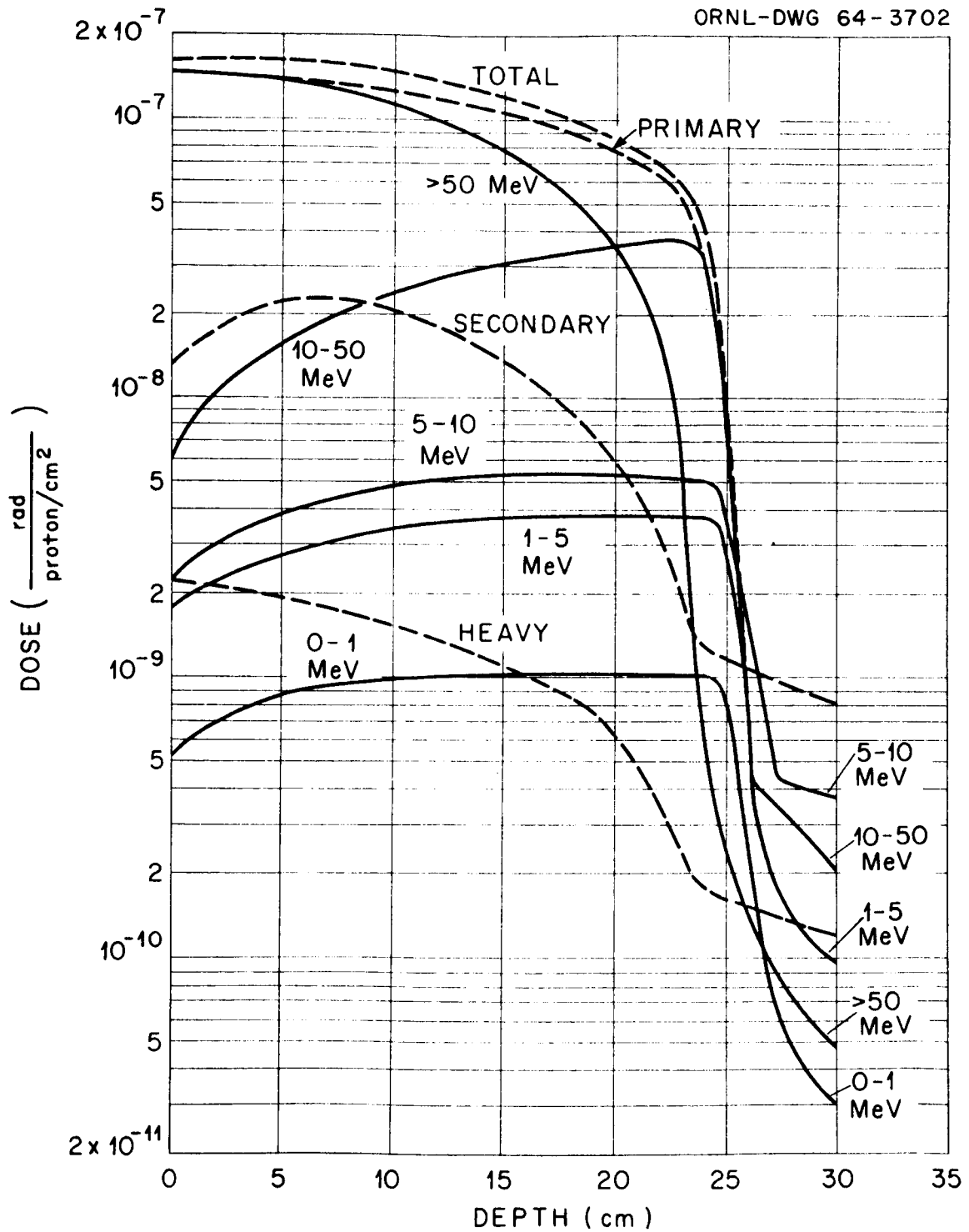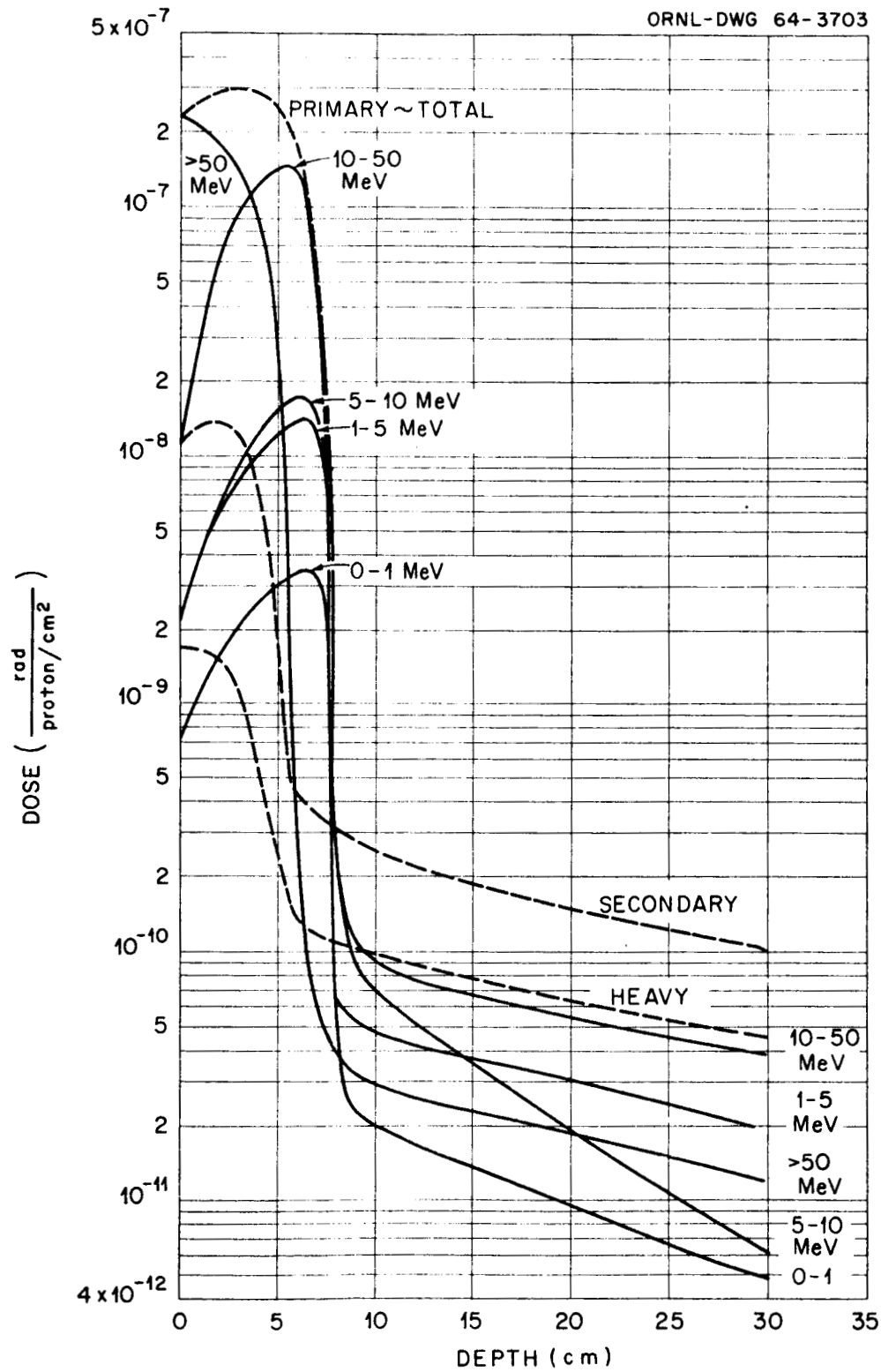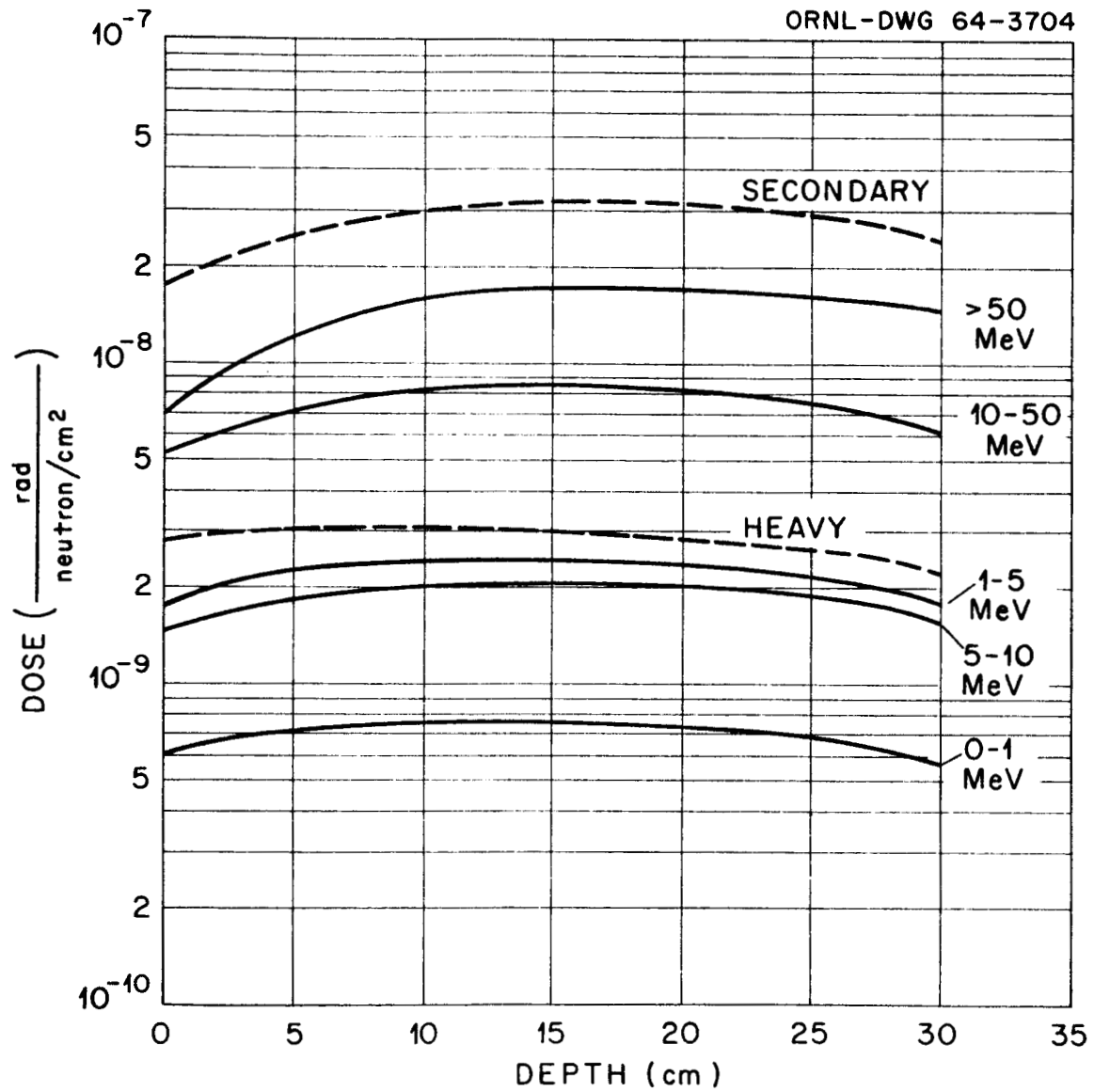Fig. A10. Rad Dose vs Depth Due To 400-MeV Isotropically Incident Protons.

ORNL-DWG 64-3701

Fig. A11. Rad Dose vs Depth Due To 300-MeV Isotropically Incident Protons.

Fig. A12. Rad Dose vs Depth Due To 200-MeV Isotropically Incident Protons.

Fig. A13. Rad Dose vs Depth Due To 100-MeV Isotropically Incident Protons.

At 200 and 100 MeV the doses still fall rapidly at a depth equal to the range of protons in tissue, but the peaks which appeared in the normally incident cases are removed since the protons reach the end of their range at different depths.

The doses due to 60-MeV isotropically incident protons are included in Table A1. Again the dose is almost entirely due to the primary ionization energy loss.

Doses resulting from isotropically incident neutrons of 400-, 300-, 200-, 100-, and 60-MeV incident energy are given in Figs. A14 through A18, respectively. The dose at the surface is not a simple factor of 2 larger than the doses due to normally incident neutrons since energy is deposited by neutrons indirectly and the secondaries build up in a complicated way.

75

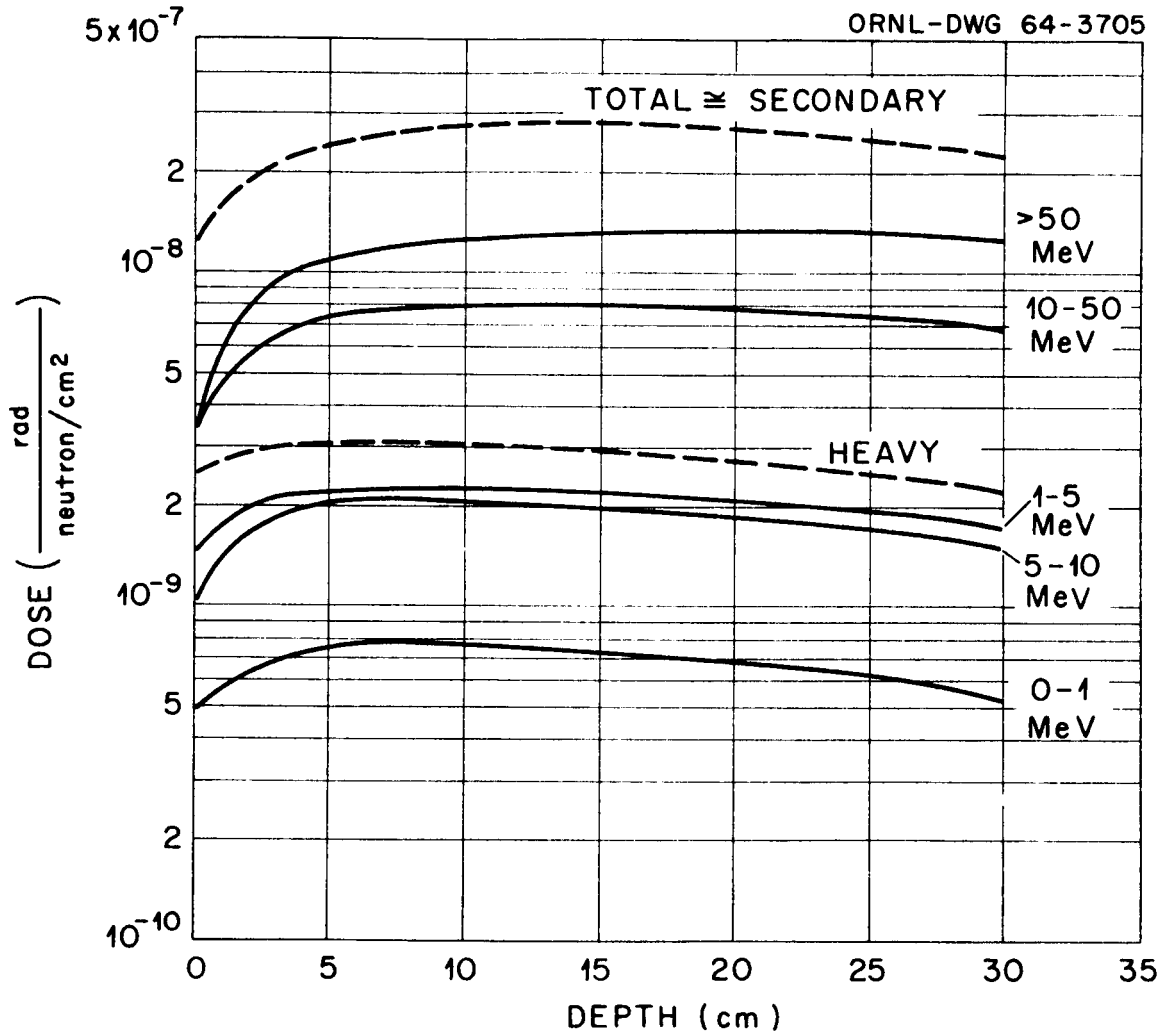Fig. A14.   Rad Dose vs Depth Due To 400-MeV Isotropically Incident Neutrons.

Fig. A15. Rad Dose vs Depth Due To 300-MeV Isotropically Incident Neutrons.
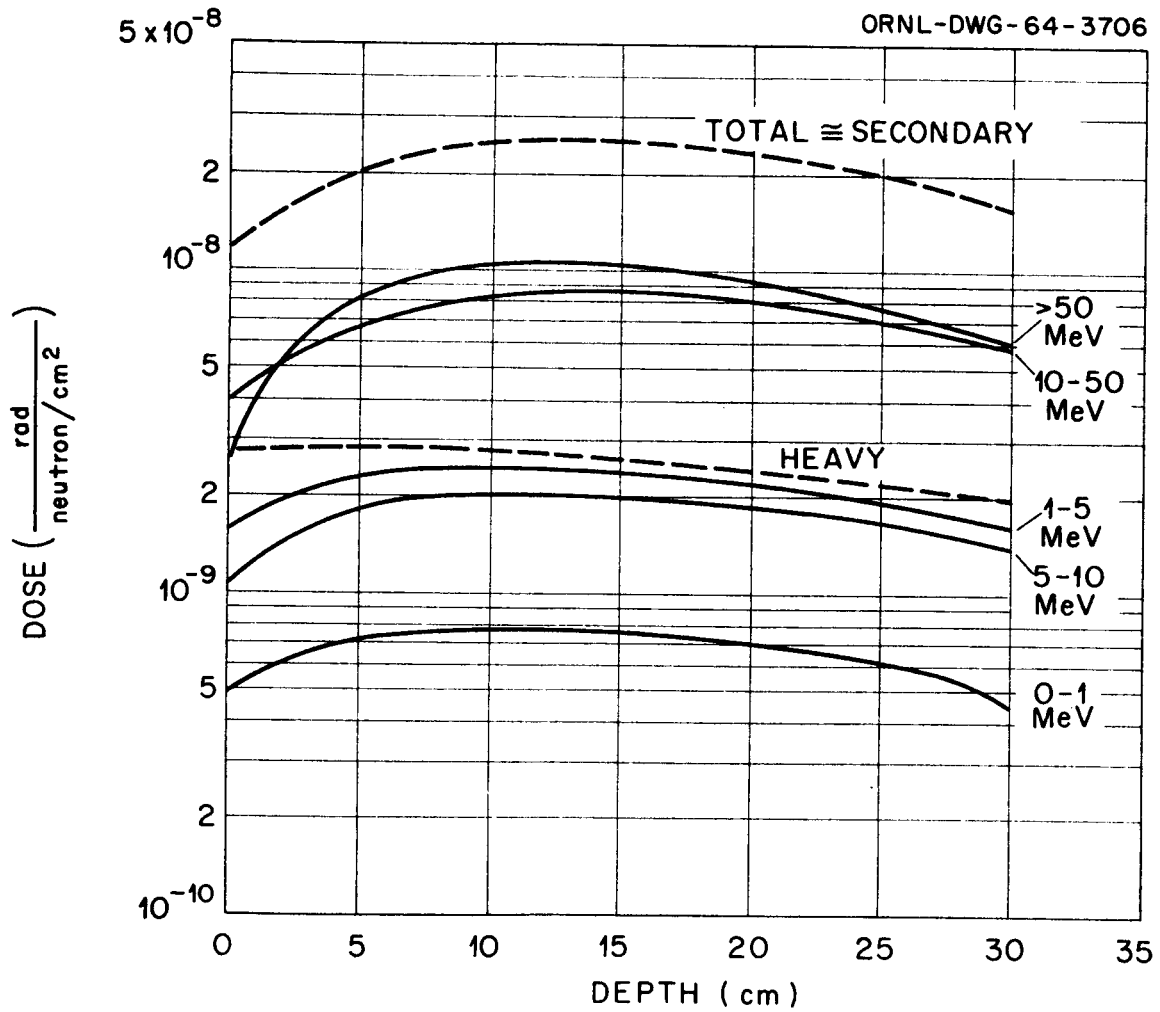
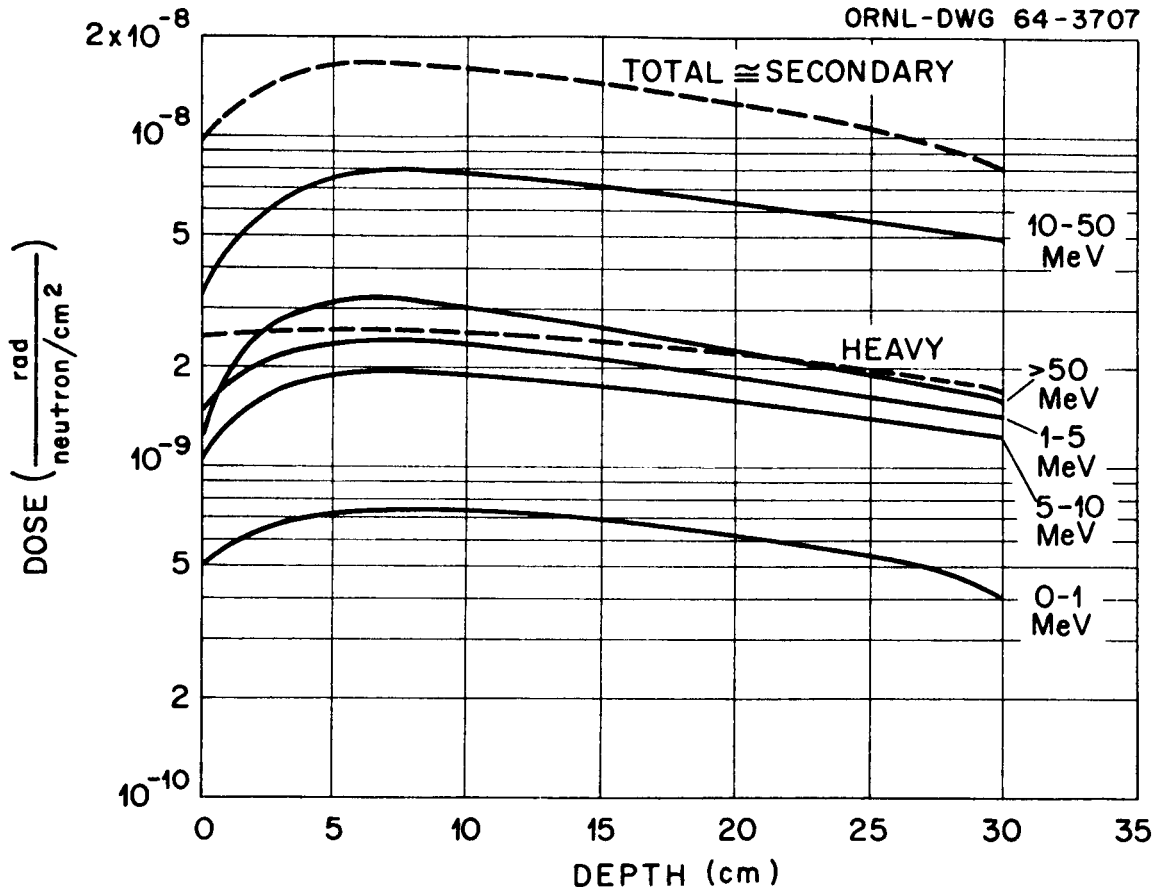Fig. A16.   Rad Dose vs Depth Due To 200-MeV Isotropically Incident Neutrons.

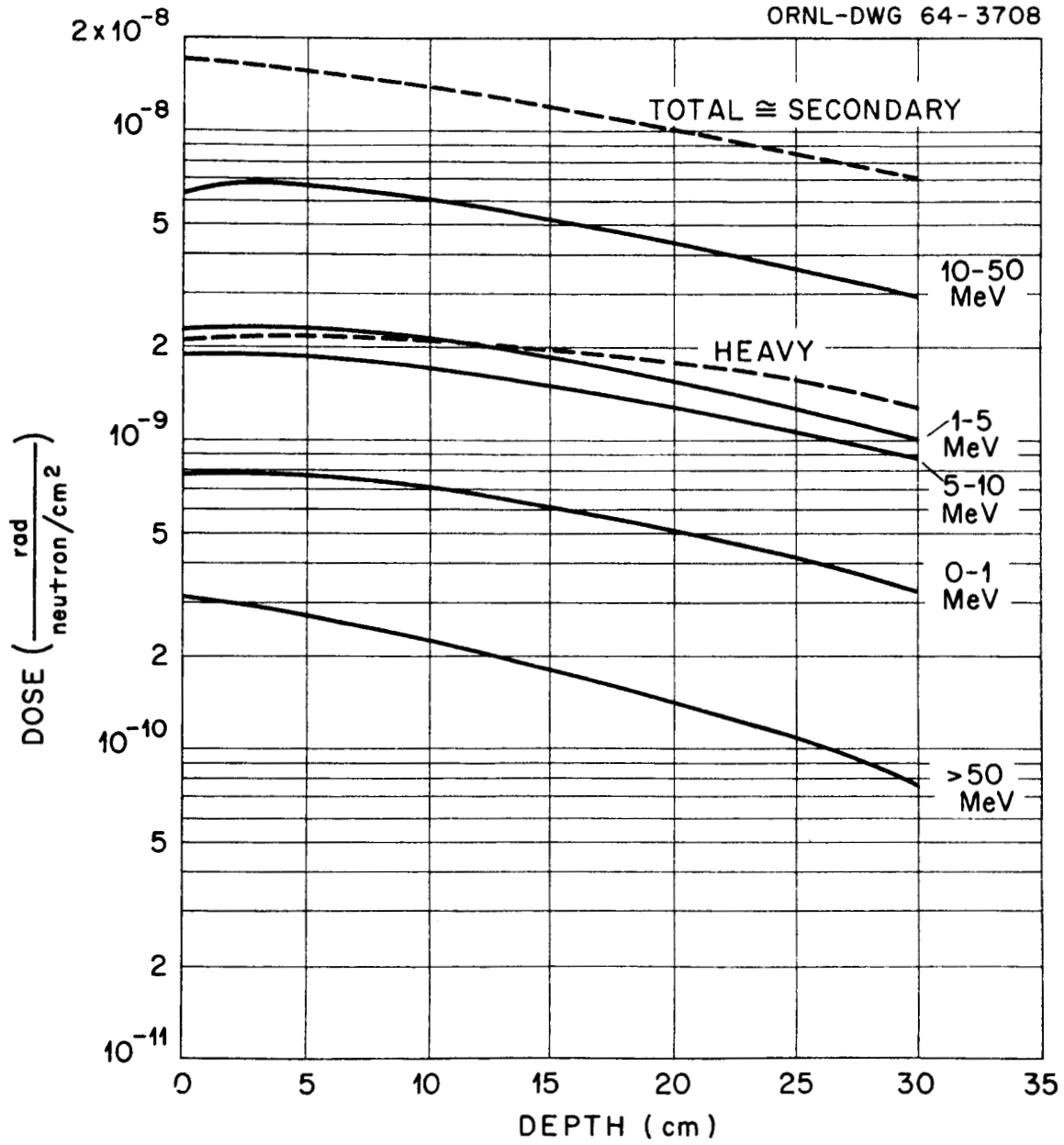Fig. A17. Rad Dose vs Depth Due to 100-MeV Isotropically Incident Neutrons.

Fig. A18. Rad Dose vs Depth Due To 60-MeV Isotropically Incident Neutrons.